IOP Publishing Physica Scripta
Phys. Scr. 95 (2020) 045205 (29pp) https://doi.org/10.1088/1402-4896/ab30e6

Modeling and study of dynamics of micro-beam coupled to two Josephson junctions

G N Koudafokê[1], C H Miwadinou[1,2], A L Hinvi[1,3], A V Monwanou[1] and J B Chabi Orou[1]

[1] Laboratoire de Mécanique des Fluides, de la Dynamique Nonlinéaire et de la Modélisation des Systèmes Biologiques (LMFDNMSB), Institut de Mathématiques et de Sciences Physiques, Porto-Novo, Bénin
[2] Département de Physiques, Ecole Normale Supérieure (ENS) Natitingou, Université Nationale des Sciences, Technologiques, Ingénierie et Mathématiques (UNSTIM) Abomey, Bénin
[3] Département des Sciences Industrielles et Techniques, IUT-Lokossa, Université Nationale des Sciences, Technologiques, Ingénierie et Mathématiques (UNSTIM) Abomey, Bénin

E-mail: clement.miwadinou@imsp-uac.org and hodevewan@yahoo.fr

Received 14 February 2019, revised 4 July 2019
Accepted for publication 10 July 2019
Published 11 February 2020

Abstract

In this work, we proposed to study the dynamics of a bi-recessed micro-beam coupled magnetically to two Josephson junctions. After building a model of micro electro mechanical systems (MEMS), the equations of their dynamics are determined. The fixed points of system are analytically checked and their stability is analyzed by using the Routh–Hurwitz criterion. For this purpose, a numerical study utilizing the bifurcation diagram, Lyapunov exponents, phase portraits and time histories is made to analyze the different dyanamic modes of micro-beam coupled to two Josephson junctions. The effect of Josephson junctions on the behavior of the micro-beam is seriously analyzed. It is obtained for each part of the MEMS the various dynamics influenced by certain parameters of the system.

Keywords: micro-beam, Josephson junctions, bifurcation, chaos, limit cycles

(Some figures may appear in colour only in the online journal)

1. Introduction

The miniaturization of technological objects has been one of the major goals of electrical engineering in recent decades. The development of tiny electrodynamic components has become an asset for achieving this goal of miniaturization. Micro electro mechanical systems (MEMS) are therefore very popular in the industrial electronics market because of their very interesting size and electrodynamic characteristics [1, 2]. The one we will study in this paper consists of two Josephson junctions as an electrical part and a bi-recessed micro-beam as its mechanical part. Roukes, Cross, Ekinci, Matheny, Kozinsky, Bullard, Vilanueva, Etaki, Herrera-May... with their collaborators have in several works [3–9] analyzed from various angles the characteristics, the properties, the dynamic, utilities and rich applications offered by these miniaturized devices. Their different and very interesting results obtained, give a great motivation for the study that we propose here by coupling a micro-beam and two Josephson junctions. On the other hand, there are several theories of beams. Here, that used is that of Euler–Bernoulli which gives the general equation of flexural vibration of the beams. This equation as used in [10, 11] will be written for a micro-beam subjected to the action of a magnetic force created by a uniform magnetic field $\vec{B}$ in the vicinity of this one. The Josephson effect since its prediction in 1962 by Brian Josephson has been the subject of an exhaustive list of scientific research. The dynamic behaviors and interesting features of the Josephson junction have been studied as in [12–17]. Being the main constituent element of the SQUID (finer magnetic field detector and RSFQ where Josephson junctions act as transistor and would allow to obtain frequencies in hundreds of GHz), the Josephson junction by its physical properties, is a device of choice for several fields of application and is therefore the subject of several studies and scientific research. For example, recently, in January 2018, Nuznetsov *et al* studied in [18] the dynamics of three and four non-identical Josephson junctions connected in series and coupled with an RLC dipole. Our

motivations for this study are also justified by the recently research on the electromechanical systems. For example, the electromechanical coupling to obtain a MEMS was done by Domguia *et al* in [10] where electrodynamic equations, stability analysis and dynamic behaviors were studied for a MEMS consisting of a micro-beam coupled to an Hindmarsh–Rose electric oscillator. Yamapi, in [19] study the harmonic dynamics and transition to chaos in a nonlinear electromechanical system with parametric coupling. They showed that the dynamics of their electromechanical system has described by an electrical Duffing oscillator coupled gyroscopically and parametrically to a linear mechanical oscillator. Recently, Yamapi and Filatrella in [20] studied the noise effect on birhythmic Josephson junction coupled to a resonator. They have found that the stability analysis of the Josephson junction coupled to a resonator shows a striking change in the birhythmic region. The attractor characterized by a frequency locked to the resonator is most stable for low bias current, when the power dissipated in the cavity is small. Ekinci and Roukes in [4] have studied the internal deformation of a nano-beam bi-embedded around its frequency of resonance and under the effect of an electromagnetic force generated by a continuous current along the length of the beam bathed in a uniform magnetic field $\vec{B}$. Other interesting parameters as the quality factor of the resonance of this miniaturized device have also been studied. For this work, we subjected the micro-beam to the same effect but with an alternating current. Inspired by all this literature we propose in this work to couple two Josephson junctions to a micro-beam immersed in an uniform magnetic field $\vec{B}$. At first, we will establish the electrodynamic equations of the MEMS; secondly, we will study the fixed points and their stabilities using the Routh–Hurwitz criterion [21] and thirdly we will evaluate the influence of each control parameter on the oscillatory dynamics of the MEMS. Considering that depending on the field of study and their applications, it is sometimes useful or undesirable many researchers are interested in the prediction of chaos and/or its control [22–27] . For this issue, we will determine the chaotic domains of our MEMS for each control parameter and will also analyze the influence of Josephson junctions on the vibratory dynamics of the micro-beam. The paper is structured as follows: section 2 gives the model and dynamics equations of the MEMS while section 3 deals with the determination of equilibrium points and their stability analysis. In section 4, the bifurcations sequences and route to chaos using the numerical simulations are analyzed and the effect of each parameter of the system is found. We provide a conclusion in the last section.

2. Model and dynamics equations of the MEMS

2.1. Presentation of the MEMS

In this work, we consider a model of MEMS as shown in figure 1 which contains a micro-beam coupled magnetically to two Josephson junctions. The presence of Josephson

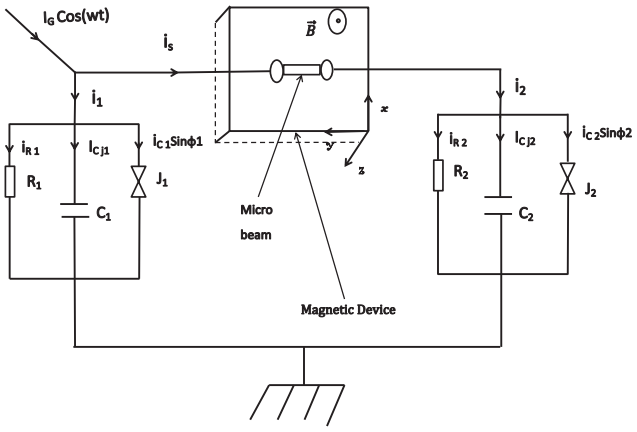

Figure 1. Electrical circuit of the MEMS where the Josephson junction is represented by its RCSJ model.

junctions due to its properties of good voltage-frequency converter. The study of the Josephson junction and its interesting features are no longer to be dismantled. Indeed, researchers such as Salem, Sastry, Abidi,… have in many of their works demonstrated the very interesting properties and characteristics of this junction [12–14, 28]. The mechanical part is a silicon flexible micro-beam covered by a metal through which the current travels and placed in a zone where magnetic field $\vec{B}$ is present.

In this paper, the symbols used are listed and defined in the following table.

Table. List of symbols and corresponding definitions

Symbols	Corresponding definitions
R_1	Resistance of the first Josephson junction
R_2	Resistance of the second Josephson junction
$\vec{B}$	The magnetic field vector
ϕ	Field flow across the lateral surface S of the beam
C_1	Self-capacitance of the first Josephson junction
C_2	Self-capacitance of the second Josephson junction
I_{C_1}	Critical current of the first Josephson junction
I_{C_2}	Critical current of the second Josephson junction
I_G	Amplitude of the excitation current
$u(z, t)$	Function characterizing transverse displacement
E	Young module of the micro-beam material
I_y	The moment of inertia of the micro-beam
ρ	Volume density of the micro-beam material
$f(t)$	The actuating force of the micro-beam
λ	Damping coefficient of the micro-beam
A	Cross-sectional area of the micro-beam
φ_1	Phase difference of first Josephson junction
φ_2	Phase difference of second Josephson junction
e_p	Electromotive force induced by the micro-beam
r_p	Electrical resistance of the micro-beam
L	Length of the micro-beam
μ	Resistivity of the micro-beam material
$\hbar$	Reduced Planck constant
e	Elementary electric charge
η_1	Normalization coefficient

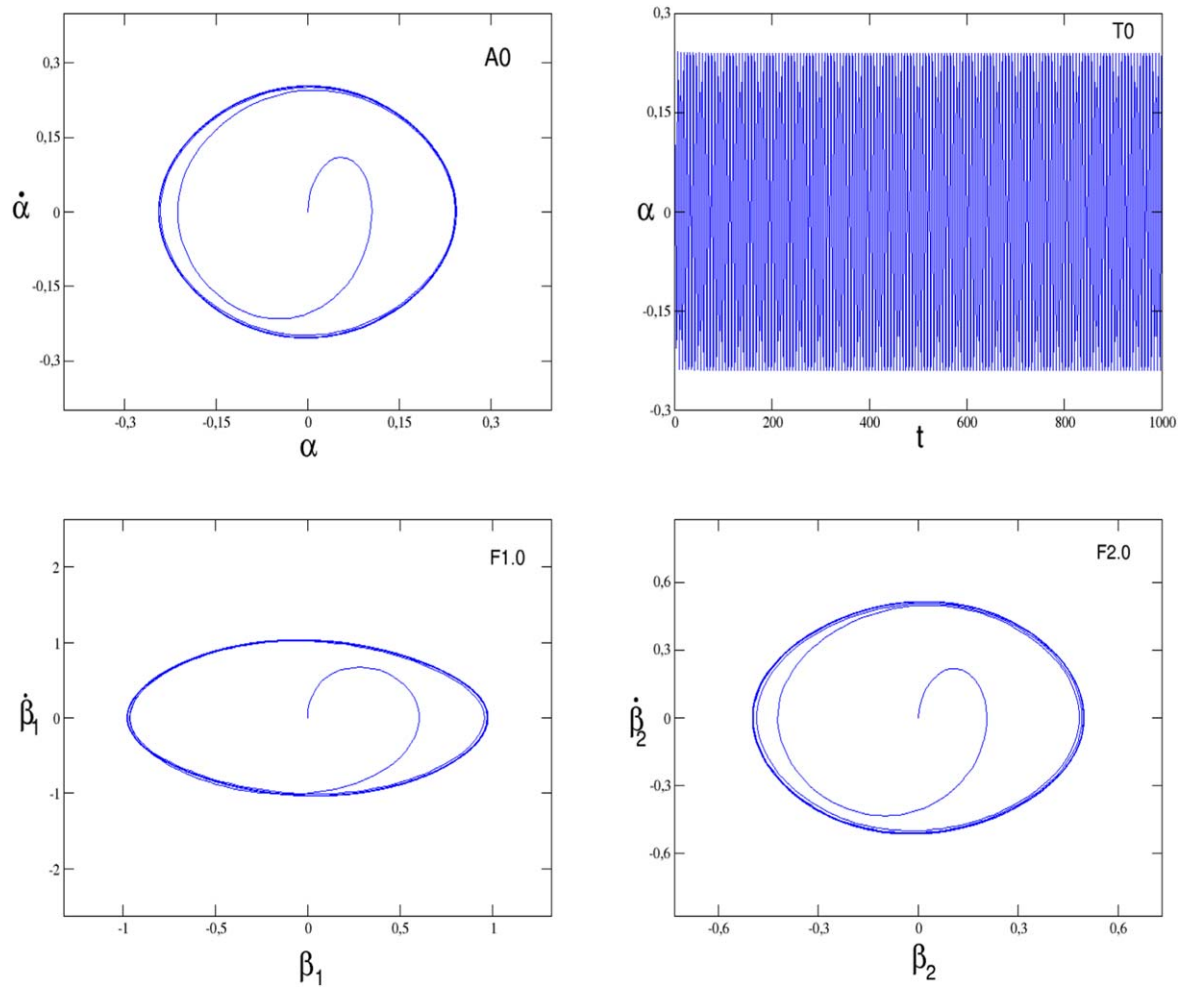

Figure 2. A0: phase space of the flexural vibration of the micro-beam; T0: time histories of the oscillations of the micro-beam; F1.0: phase difference phase space of the first Josephson junction; F2.0: phase difference phase space of the second Josephson junction; A_0: $\dot{\alpha} = f(\alpha)$; T_0: $\alpha = f(t)$; F1.0: $\dot{\beta}_1 = f(\beta_1)$ and F2.0: $\dot{\beta}_2 = f(\beta_2)$; $\omega_0 = 1$; $i_{G_0} = 2$; $J_1 = 1$; $J_2 = 3$; $J_3 = -1.6$; $J_4 = 2$; $\varphi_{0_1} = 1$; $\varphi_{0_2} = 0.5$; $\sigma_1 = 1$; $\sigma_2 = 2$; $\sigma_3 = 1$; $\sigma_4 = 2$; $\varepsilon_1 = 1.5$; $\varepsilon_2 = 0.9$; $\varepsilon_3 = 0.5$.

2.2. Mathematical modeling of the system

We consider the schematic diagram of MEMS (figure 1) under consideration in this work and we apply the node law. The exited current is written as

$$I_G \cos wt = i_1 + i_s. \tag{1}$$

The equations of the electrical part where the Josephson junction is represented by its RCSJ model [14, 17] are written:

$$i_1 = \frac{\hbar C_1}{2e}\frac{\mathrm{d}^2\varphi_1}{\mathrm{d}t^2} + \frac{\hbar}{2\,e\,R_1}\frac{\mathrm{d}\varphi_1}{\mathrm{d}t} + I_{C_1}\sin\varphi_1 = I_G\cos(wt) - i_s, \tag{2}$$

and

$$i_s = i_2 = \frac{\hbar\ C_2}{2\,e}\frac{\mathrm{d}^2\varphi_2}{\mathrm{d}t^2} + \frac{\hbar}{2\,e\,R_2}\frac{\mathrm{d}\varphi_2}{\mathrm{d}t} + I_{C_2}\sin\varphi_2. \tag{3}$$

Considering the mesh $(R_1\,R_2\,R_1)$ we can write

$$R_1 \cdot i_{R_1} - (r_p \cdot i_s - e_p) - R_2 \cdot i_{R_2} = 0,$$

which can be rewritten as follows

$$\frac{\hbar\ R_1}{2\,e\,R_1}\frac{\mathrm{d}\varphi_1}{\mathrm{d}t} - r_p i_s + e_p - \frac{\hbar\ R_2}{2\,e\,R_2}\frac{\mathrm{d}\varphi_2}{\mathrm{d}t} = 0.$$

Thus

$$i_s = \frac{\hbar}{2\,e\,r_p}(\dot{\varphi}_1 - \dot{\varphi}_2) + \frac{e_p}{r_p},$$

with $\left(\frac{e_p}{r_p}\right)$ current induced by current flow through the magnetic field. $I_{C_1}\sin\varphi_1$ and $I_{C_2}\sin\varphi_2$ designate the current through the first intrinsic junction and the current through the second intrinsic junction. Replacing i_s by its expression in

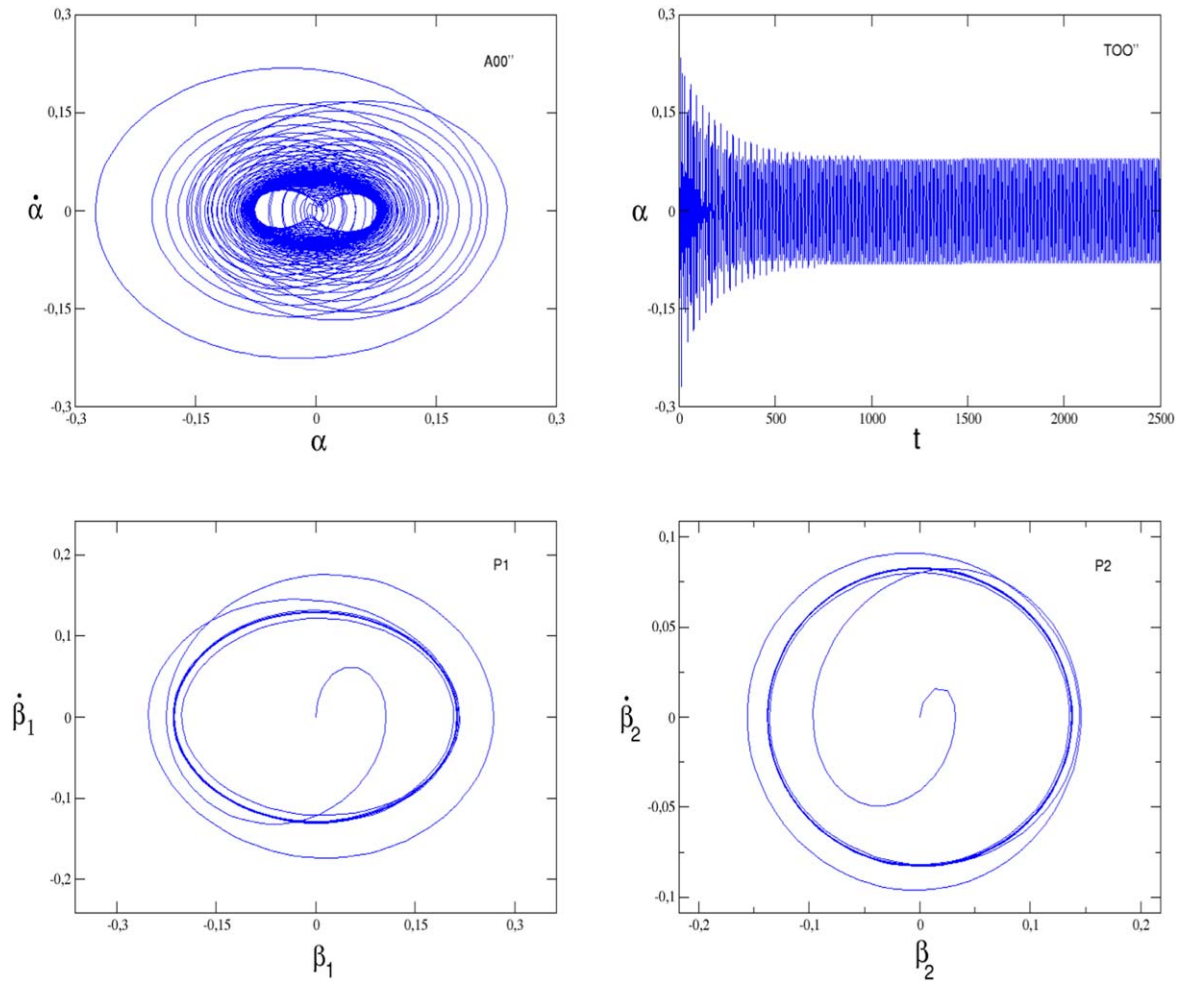

Figure 3. A00″: phase space of the flexural vibration of the micro-beam; T00″: time histories of the oscillations of the micro-beam; P1: phase difference phase space of the first Josephson junction; P2: phase difference phase space of the second Josephson junction; $\omega_0 = 0.6$; $i_{G_0} = 0.08$; $J_1 = 0.25$; $J_2 = 0.39$; $J_3 = 0.26$; $J_4 = 10^{-4}$; $\varphi_{0_1} = \frac{2\pi}{3}$; $\varphi_{0_2} = \frac{\pi}{6}$; $\sigma_1 = 0.26$; $\sigma_2 = 0.38$; $\sigma_3 = 0.24$; $\sigma_4 = 10^{-4}$; $\varepsilon_1 = 10^{-2}$; $\varepsilon_2 = 1$; $\varepsilon_3 = 0.22$.

equations (2) and (3) we get:

$$\ddot{\varphi_1} + \frac{R_1 + r_p}{R_1 r_p C_1}\dot{\varphi_1} + \frac{2eI_{C_1}}{\hbar C_1}\sin\varphi_1 - \frac{1}{r_p C_1}\dot{\varphi_2} + \frac{2e}{\hbar C_1 r_p}e_p = \frac{2eI_G}{\hbar C_1}\cos(\omega t), \tag{4}$$

$$\ddot{\varphi_2} + \frac{R_2 + r_p}{R_2 r_p C_2}\dot{\varphi_2} + \frac{2eI_{C_2}}{\hbar C_2}\sin\varphi_1 - \frac{1}{r_p C_2}\dot{\varphi_1} - \frac{2e}{\hbar C_2 r_p}e_p = 0. \tag{5}$$

According to the differential equation of the dynamics of micro beams [10, 11], the mechanical part equation is written:

$$E.I_y\frac{\partial^4 u(z,t)}{\partial z^4} + \rho A\frac{\partial^2 u(z,t)}{\partial t^2} + \lambda\frac{\partial u(z,t)}{\partial t} + NLT = f(t). \tag{6}$$

In this study it is assumed that $NLT = 0$.

The actuating force $f(t)$ of the beam is a Lorentz force (magnetic) and is written:

$$f(t) = I_C.\,B.\,l\,\sin(\vec{B},\vec{l}) = B\,i_s = B\left[\frac{\hbar}{2\,e\,r_p}(\dot{\varphi_1} - \dot{\varphi_2}) + \frac{e_p}{r_p}\right]. \tag{7}$$

Inserting equation (7) into equation (6) we obtain:

$$E.I_y\frac{\partial^4 u(z,t)}{\partial z^4} + \rho A\frac{\partial^2 u(z,t)}{\partial t^2} + \lambda\frac{\partial u(z,t)}{\partial t} = B\left[\frac{\hbar}{2er_p}(\dot{\varphi_1} - \dot{\varphi_2}) + \frac{e_p}{r_p}\right]. \tag{8}$$

Let ϕ the field flow across the lateral surface S of the beam. Thus

$$\phi = BS,$$

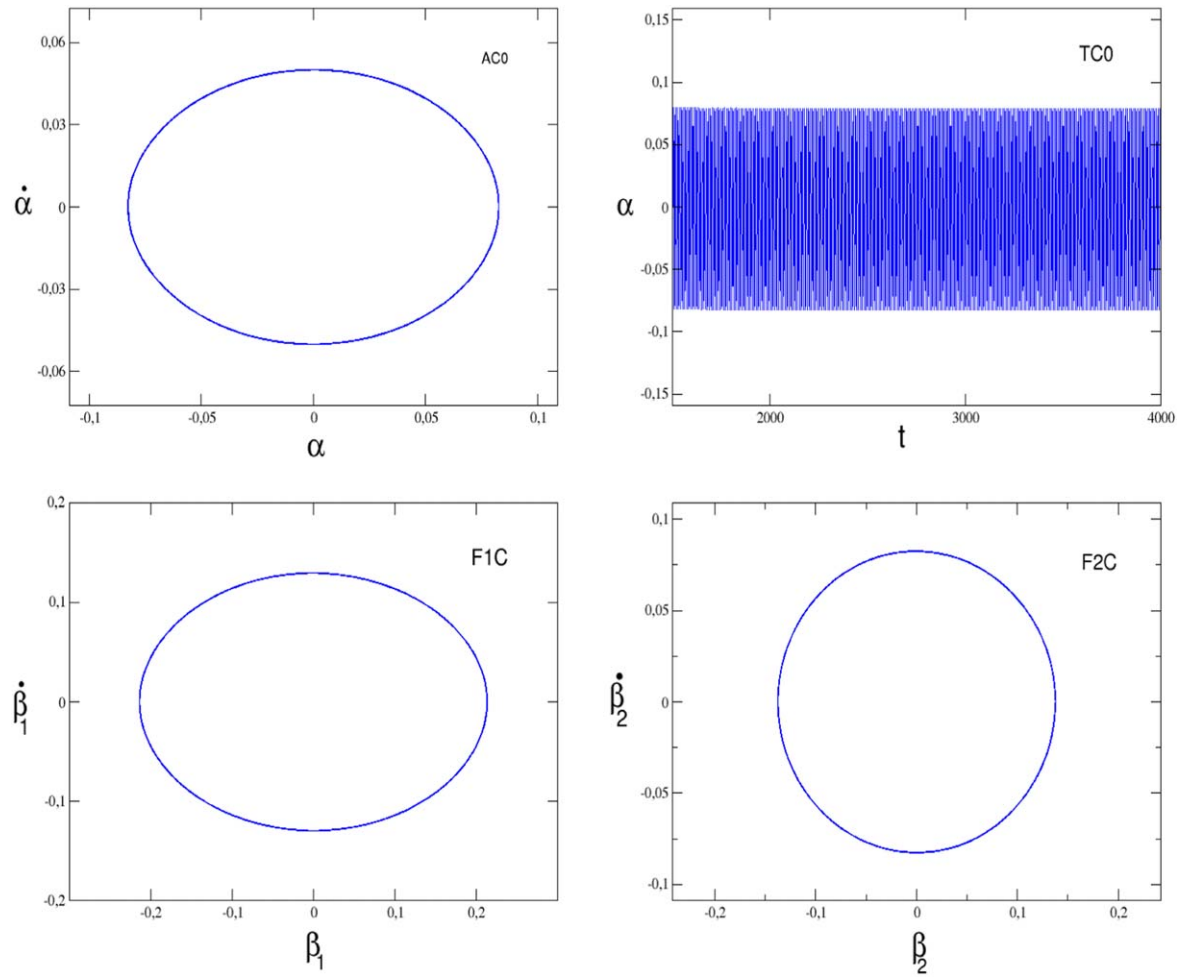

Figure 4. ACO: phase space of the flexural vibration of the micro-beam; TCO: time histories of the oscillations of the micro-beam; F1C: phase difference phase space of the first Josephson junction; F2C: phase difference phase space of the second Josephson junction; $\omega_0 = 0.6$; $i_{G_0} = 0.08$; $J_1 = 0.25$; $J_2 = 0.39$; $J_3 = 0.26$; $J_4 = 10^{-4}$; $\varphi_{0_1} = \frac{2\pi}{3}$; $\varphi_{0_2} = \frac{\pi}{6}$; $\sigma_1 = 0.26$; $\sigma_2 = 0.38$; $\sigma_3 = 0.24$; $\sigma_4 = 10^{-4}$; $\varepsilon_1 = 10^{-2}$; $\varepsilon_2 = 1$; $\varepsilon_3 = 0.22$.

with $S = 2\int_o^L u(z, t)\mathrm{d}z$, and we have

$$e_p = -2\,B\int_o^L \frac{\partial u(z, t)}{\partial t}\mathrm{d}z \qquad \text{and}$$

$$(e_p/r_p) = \frac{-2\,B\,A}{\mu\,L}\int_o^L \frac{\partial u(z, t)}{\partial t}\mathrm{d}z.$$

The shape of the modes must satisfy the differential geometries and boundary conditions [29]. The deflection $u(z, t)$ of the beam can then be written as follows:

$$u(z, t) = \sum_{n=1}^{\infty} Z_n(z)\,T_n(t),$$

where n indicates the mode of vibration; $T_n(t)$ represents the generalized coordinate of the amplitudes and $Z_n(z)$ the set eigenfunctions of the equation:

$$\frac{\partial^4 u(z, t)}{\partial z^4} + \frac{\rho A}{E.I_y}\frac{\partial^2 u(z, t)}{\partial t^2} = 0.$$

In our case we have $u(0, t) = u(L, t) = 0$ (boundary conditions) and the set eigenfunctions $Z_n(z)$ are written:

$$Z_n(z) = a_n(\cos\xi_n z - \cosh\xi_n z) + b_n(\sin\xi_n z - \sinh\xi_n z),$$

with ξ_n the solution of the transcendental equation:

$$\cos\xi_n L\cosh\xi_n L - 1 = 0.$$

As we focus on the study of the ground state we will take it for the rest $n = 1$.

By doing the standardization below :

$$\int_0^L Z_1(z)Z_n(z)\mathrm{d}z = L^3\delta_{1,n} = \begin{cases} L^3 & \text{if} \quad n = 1 \\ 0 & \text{if} \quad n \neq 1 \end{cases} \tag{9}$$

and let us put $\eta_1 = \frac{1}{L^2}\int_0^L Z_1(z)\mathrm{d}z$ and bringing all the above transformations to the equations (4), (5) and (8) we get:

$$\ddot{\varphi_1} + \frac{R_1 + r_p}{R_1 r_p C_1}\dot{\varphi_1} + \frac{2eI_{C_1}}{\hbar C_1}\sin\varphi_1 - \frac{1}{r_p C_1}\dot{\varphi_2} - \frac{4eBAL\eta_1}{\hbar C_1\mu}\dot{T} = \frac{2eI_G}{\hbar C_1}\cos(\omega t), \tag{10}$$

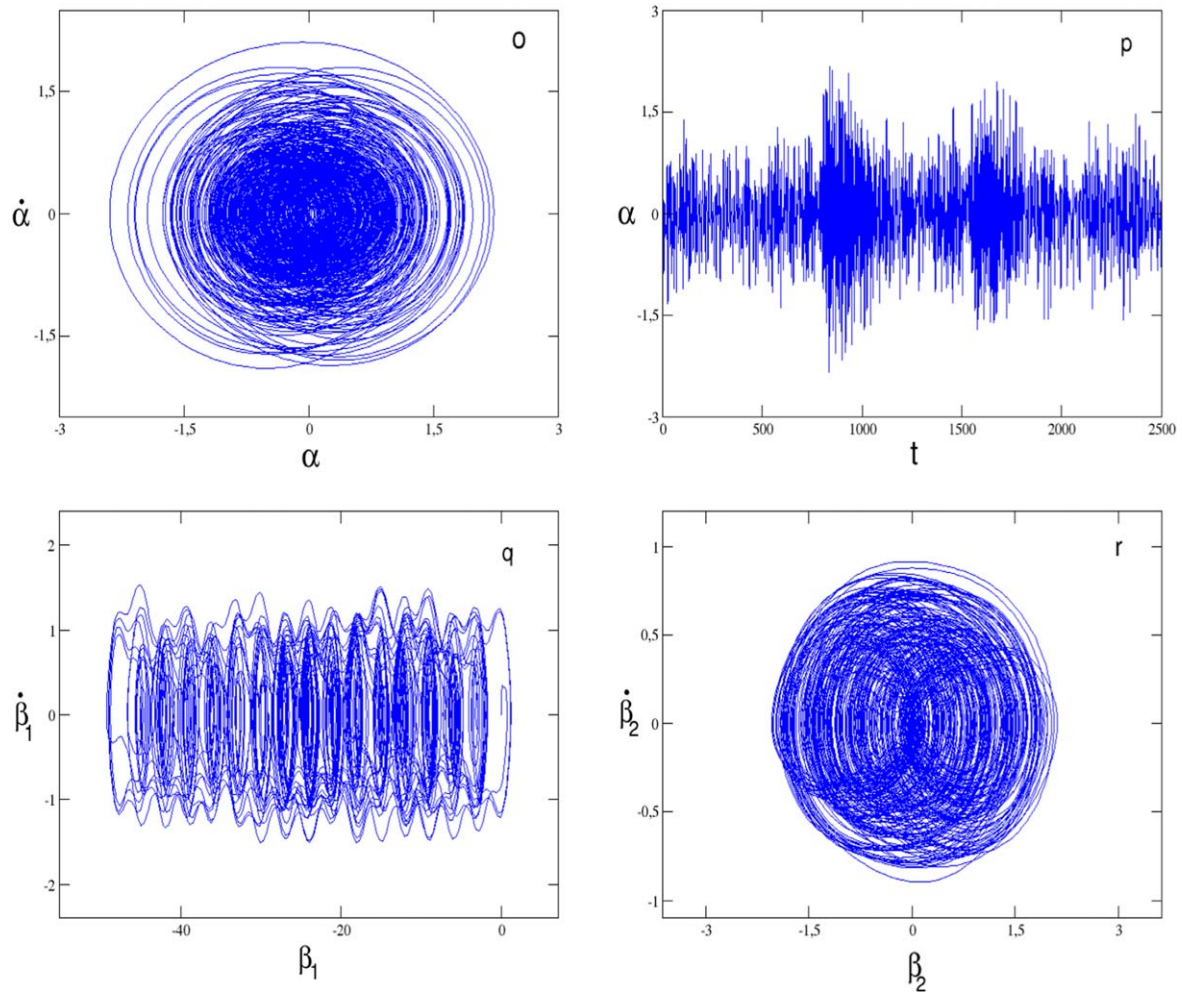

Figure 5. o: phase space of the flexural vibration of the micro-beam; p: time histories of the oscillations of the micro-beam; q: phase difference phase space of the first Josephson junction; r: phase difference phase space of the second Josephson junction; $\omega_0 = 0.6$; $i_{G_0} = 0.5$; $J_1 = 0.25$; $J_2 = 0.39$; $J_3 = 0.26$; $J_4 = 10^{-4}$; $\varphi_{0_1} = \frac{2\pi}{3}$; $\varphi_{0_2} = \frac{\pi}{6}$; $\sigma_1 = 0.26$; $\sigma_2 = 0.38$; $\sigma_3 = 0.24$; $\sigma_4 = 10^{-4}$; $\varepsilon_1 = 10^{-2}$; $\varepsilon_2 = 1$; $\varepsilon_3 = 0.22$.

$$\ddot{\varphi_2} + \frac{R_2 + r_p}{R_2 r_p C_2}\dot{\varphi_2} + \frac{2eI_{C_2}}{\hbar C_2}\sin\varphi_1 - \frac{1}{r_p C_2}\dot{\varphi_1} + \frac{4eBAL\eta_1}{\hbar C_2 \mu}\dot{T} = 0, \tag{11}$$

and

$$\rho\, A\, \ddot{T}(t)Z_1(z) + \lambda\, \dot{T}(t)Z_1(z) + E.I_y\, \xi^4 T(t)Z_1(z) + \frac{B\,\hbar}{2\,e\,r_p}(\dot{\varphi_2} - \dot{\varphi_1}) + \frac{2\,B^2\,A}{\mu\,L}\,\dot{T}(t)\int_o^L Z_1(z)\mathrm{d}z = 0.$$

Better we have:

$$\rho\, A\, \ddot{T}(t)Z_1(z) + \lambda\, \dot{T}(t)Z_1(z) + E.I_y\, \xi^4 T(t)Z_1(z) + \frac{B\,\hbar}{2\,e\,r_p}(\dot{\varphi_2} - \dot{\varphi_1}) + \frac{2\,B^2\,A\,\eta_1\,L}{\mu}\,\dot{T}(t) = 0. \tag{12}$$

By integrating the equation (12) with $\int_o^L Z_1(z)\mathrm{d}z$ and considering the normalization above we have:

$$\ddot{T}(t) + \left(\frac{\lambda}{\rho\, A} + \frac{2\,B^2\,\eta_1^2}{\mu\rho}\right)\dot{T}(t) + \frac{E.I_y\,\xi^4}{\rho\, A}T(t) + \frac{B\,\hbar\eta_1}{2\,e\,\rho\,A\,r_p\,L}(\varphi_2 - \dot{\varphi_1}) = 0 \tag{13}$$

Let:

$$\tau = \omega_1\, t; \quad \beta_1 = \frac{\varphi_1}{\varphi_{0_1}}; \quad \beta_2 = \frac{\varphi_2}{\varphi_{0_2}} \quad \text{and} \quad \alpha = \frac{T}{T_0}.$$

The dimensionless equations are then written:

$$\ddot{\alpha} = -\varepsilon_1\dot{\alpha} - \varepsilon_2\alpha - \varepsilon_3[\varphi_{0_2}\,\dot{\beta_2} - \varphi_{0_1}\,\dot{\beta_1}], \tag{14}$$

$$\ddot{\beta_1} = -J_1\dot{\beta_1} - J_2\sin(\varphi_{0_1}\beta_1) + J_3\,\dot{\beta_2} + J_4\,\dot{\alpha} + i_{G_0}\cos(\omega_0\tau), \tag{15}$$

$$\ddot{\beta_2} = -\sigma_1\,\dot{\beta_2} - \sigma_2\sin(\varphi_{0_2}\beta_2) + \sigma_3\dot{\beta_1} - \sigma_4\,\dot{\alpha}, \tag{16}$$

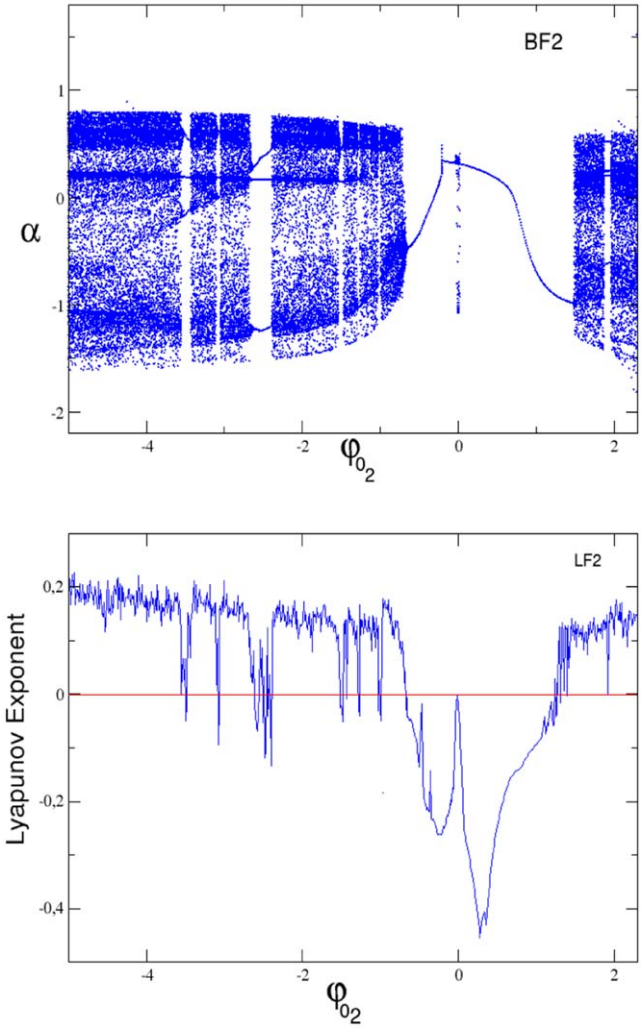

Figure 6. BF2: bifurcation diagram; LF2: Lyapunov exponent; $\omega_0 = 1$; $i_{G_0} = 2$; $J_1 = 1$; $J_2 = 3$; $J_3 = -1.6$; $J_4 = 2$; $\varphi_{0_1} = 1$; $\sigma_1 = 1$; $\sigma_2 = 2$; $\sigma_3 = 1$; $\sigma_4 = 2$; $\varepsilon_1 = 1.5$; $\varepsilon_2 = 0.9$; $\varepsilon_3 = 0.5$.

with:

$$J_1 = \frac{R_1 + r_p}{R_1\, r_p\, C_1\, \omega_1}; \quad J_2 = \frac{2\, e\, I_{C_1}}{\hbar\ C_1\, \omega_1^2\, \varphi_{0_1}};$$

$$J_3 = \frac{\varphi_{0_2}}{r_p\, C_1\, \omega_1\, \varphi_{0_1}}; \quad J_4 = \frac{4\, e\, B\, A\, L\, \eta_1\, T_0}{\hbar\ C_1\, \mu\, \omega_1\, \varphi_{0_1}}$$

$$i_{G_0} = \frac{2\, e\, I_G}{\hbar\ C_1\, \omega_1^2\, \varphi_{0_1}}; \quad \omega_0 = \frac{\omega}{\omega_1};$$

$$\sigma_1 = \frac{R_2 + r_p}{R_2\, r_p\, C_2\, \omega_1}; \quad \sigma_2 = \frac{2\, e\, I_{C_2}}{\hbar\ C_2\, \omega_1^2\, \varphi_{0_2}};$$

$$\sigma_3 = \frac{\varphi_{0_1}}{r_p\, C_2\, \omega_1\, \varphi_{0_2}}; \quad \sigma_4 = \frac{4\, e\, B\, A\, L\, \eta_1\, T_0}{\hbar\ C_2\, \mu\omega_1\, \varphi_{0_2}};$$

$$\varepsilon_1 = \left(\frac{\lambda}{\rho\, A\, \omega_1} + \frac{2\, B^2\eta_1^2}{\rho\, \omega_1\, \mu}\right);$$

$$\varepsilon_2 = \frac{E\, I_y\, \xi^4}{\rho\, A\, \omega_1^2}; \quad \varepsilon_3 = \frac{B\, \hbar\ \eta_1}{2\, e\, \rho\, A\, r_p\, L\, \omega_1\, T_0}.$$

The micro electromechanical system shown in figure 1 is described by equations (14)–(16). In this work, σ_3, ε_3, and J_1 are the damping coefficients of the phase difference ϕ_1 of the first Josephson junction; σ_1, ε_1, and J_3 are the damping coefficients of the phase difference ϕ_2 of the second Josephson junction; σ_4, ε_1, and J_4 are the damping coefficients of the micro-beam; ε_2 the pulsation of the micro-beam; J_2 the coefficient of intrinsic current through the first Josephson junction; σ_2 the coefficient of intrinsic current through second Josephson junction; ω_0 the frequency of the excitation current; i_{G_0} the amplitude of the excitation current; φ_{0_1} initial phase of the first Josephson junctionϕ_1; φ_{0_2} initial phase of the second Josephson junction

3. Fixed points and stability

In this section, we search the equilibrium points of the autonomous system and we analyze their stability. For this end, the autonomus system can been written as:

$$\begin{aligned}
\dot{\alpha} &= x\\
\dot{x} &= -\varepsilon_1 x - \varepsilon_2\alpha - \varepsilon_3(\varphi_{0_2}\, z - \varphi_{0_1}\, y)\\
\dot{\beta_1} &= y\\
\dot{y} &= -J_1 y - J_2\, \sin(\varphi_{0_1}\beta_1) + J_3 z + J_4\, x\\
\dot{\beta_2} &= z\\
\dot{z} &= -\sigma_1\, z - \sigma_2\, \sin(\varphi_{0_2}\beta_2) + \sigma_3 y - \sigma_4\, x. \qquad (17)
\end{aligned}$$

Thus the fixed points of the system are defined by:

$$E^*(\alpha^*, x^*, \beta_1^*, y^*, \beta_2^*, z^*) = \left(0, 0, \frac{k_1\pi}{\varphi_{0_1}}, 0, \frac{k_2\pi}{\varphi_{0_2}}, 0\right)$$

$$k_i, \in Z.$$

At the fixed point E^*, the Jacobian is:

$$J(E^*) = \begin{bmatrix}
0 & 1 & 0 & 0 & 0 & 0\\
-\varepsilon_2 & -\varepsilon_1 & 0 & \varepsilon_3\, \varphi_{0_1} & 0 & -\varepsilon_3\, \varphi_{0_2}\\
0 & 0 & 0 & 1 & 0 & 0\\
0 & J_4 & -J_2\, \varphi_{0_1}\cos(k_1\pi) & -J_1 & 0 & J_3\\
0 & 0 & 0 & 0 & 0 & 1\\
0 & -\sigma_4 & 0 & \sigma_3 & -\sigma_2\, \varphi_{0_2}\cos(k_2\pi) & -\sigma_1
\end{bmatrix}.$$

The characteristic equation at E^* is:

$$\kappa^6 + \mu_6\kappa^5 + \mu_5\kappa^4 + \mu_4\, \kappa^3 + \mu_3\, \kappa^2 + \mu_2\, \kappa + \mu_1 = 0 \qquad (18)$$

with:

$$\mu_1 = \varepsilon_2 J_2\, \varphi_{0_1}\sigma_2\varphi_{0_2}\cos(k_1\pi)\cos(k_2\pi),$$

$$\mu_2 = \sigma_1\varepsilon_2 J_2\, \varphi_{0_1}\cos(k_1\pi) + \sigma_2\varepsilon_2 J_1\, \varphi_{0_2}\cos(k_2\pi) + \varepsilon_1 J_2\, \varphi_{0_1}\sigma_2\varphi_{0_2}\cos(k_1\pi)\cos(k_2\pi),$$

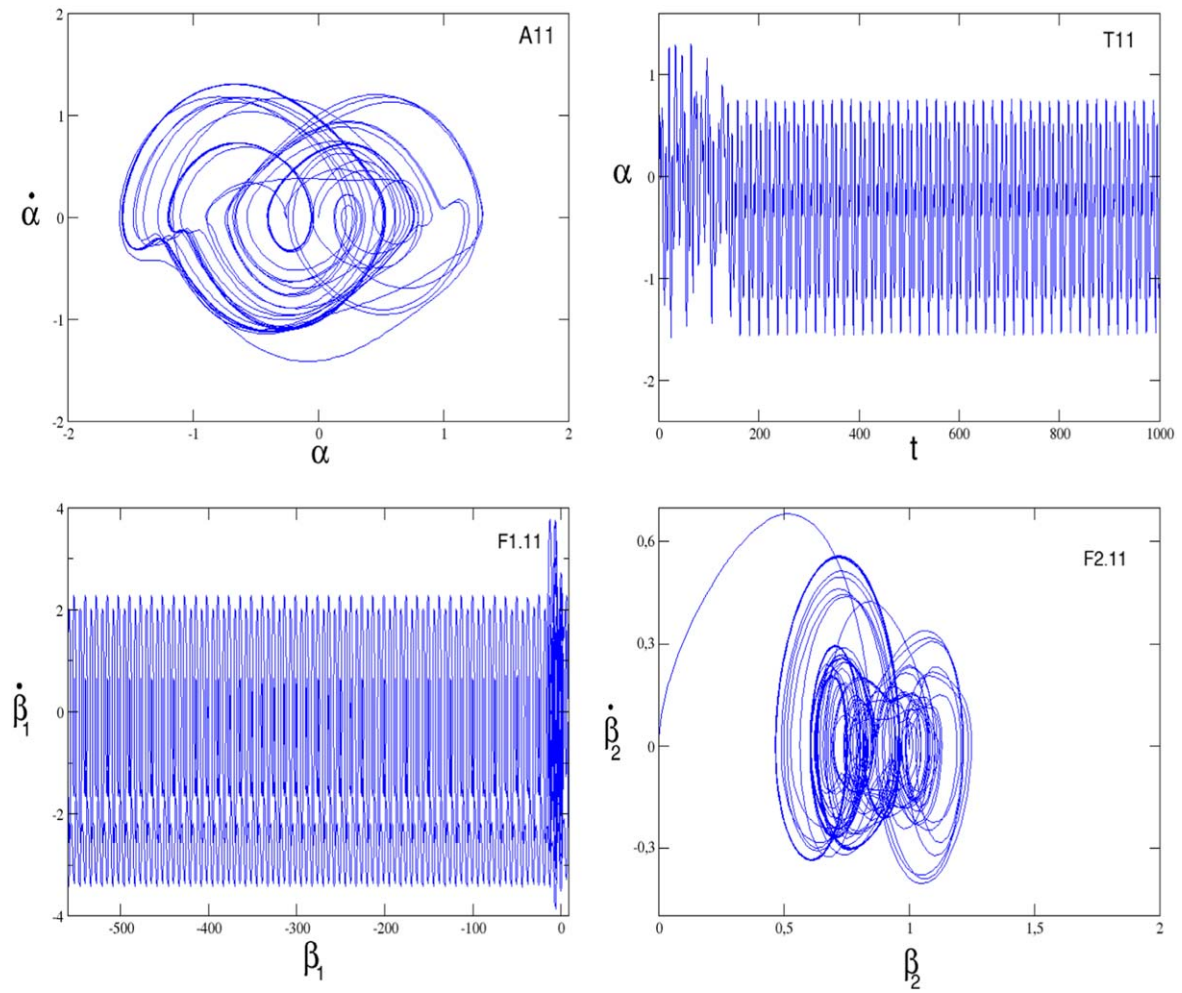

Figure 7. A_{11}: phase space of the flexural vibration of the micro-beam; T_{11}: time histories of the oscillations of the micro-beam; $F1_{11}$: phase difference phase space of the first Josephson junction; $F2_{11}$: phase difference phase space of the second Josephson junction; $\omega_0 = 1$; $i_{G_0} = 2$; $J_1 = 1$; $J_2 = 3$; $J_3 = -1.6$; $J_4 = 2$; $\varphi_{0_1} = 1$; $\varphi_{0_2} = -3.494$; $\sigma_1 = 1$; $\sigma_2 = 2$; $\sigma_3 = 1$; $\sigma_4 = 2$; $\varepsilon_1 = 1.5$; $\varepsilon_2 = 0.9$; $\varepsilon_3 = 0.5$.

$$\begin{aligned}\mu_3 = {} & \varepsilon_2 J_1 \sigma_1 + \sigma_1 \varepsilon_1 J_2 \varphi_{0_1} \cos(k_1\pi) + \sigma_2 \varepsilon_1 J_1 \varphi_{0_2} \cos(k_2\pi) \\ & + J_2 \varphi_{0_1} \sigma_2 \varphi_{0_2} \cos(k_1\pi)\cos(k_2\pi) \\ & - \varepsilon_3 \varphi_{0_1} J_4 \sigma_2 \varphi_{0_2} \cos(k_2\pi) + \varepsilon_2 \sigma_2 \varphi_{0_2} \cos(k_2\pi) \\ & - \varepsilon_2 J_3 \sigma_3 - \varepsilon_3 \varphi_{0_2} \sigma_4 J_2 \varphi_{0_1} \cos(k_1\pi) + \varepsilon_2 J_2 \varphi_{0_1} \cos(k_1\pi),\end{aligned}$$

$$\begin{aligned}\mu_4 = {} & \varepsilon_1 \sigma_1 J_1 + \sigma_1 J_2 \varphi_{0_1} \cos(k_1\pi) - \varepsilon_3 \varphi_{0_1} J_4 \sigma_1 \\ & + \varepsilon_2 \sigma_1 + J_1 \sigma_2 \varphi_{0_2} \cos(k_2\pi) + \varepsilon_1 \sigma_2 \varphi_{0_2} \cos(k_2\pi) \\ & - \varepsilon_1 J_3 \sigma_3 + \varepsilon_3 \varphi_{0_2} J_4 \sigma_3 + \varepsilon_3 \varphi_{0_1} J_3 \sigma_4 \\ & - \varepsilon_3 \varphi_{0_2} J_1 \sigma_4 + \varepsilon_2 J_1 + \varepsilon_1 J_2 \varphi_{0_1} \cos(k_1\pi),\end{aligned}$$

$$\begin{aligned}\mu_5 = {} & J_1 \sigma_1 + \varepsilon_1 \sigma_1 + \sigma_2 \varphi_{0_2} \cos(k_2\pi) - J_3 \sigma_3 \\ & - \varepsilon_3 \varphi_{0_2} \sigma_4 + \varepsilon_1 J_1 + J_2 \varphi_{0_1} \cos(k_1\pi) - \varepsilon_3 \varphi_{0_1} J_4 + \varepsilon_2,\end{aligned}$$

$$\mu_6 = \sigma_1 + J_1 + \varepsilon_1.$$

Utilizing the Routh–Hurwitz criterion [21], the stability condition is reduced as follows:

$$R_{\text{th}_1} = \mu_6 > 0,$$

$$R_{\text{th}_2} = \mu_6\,\mu_5 - \mu_4 > 0,$$

$$R_{\text{th}_3} = -\mu_4^2 + \mu_2\,\mu_6 + \mu_4\mu_5\mu_6 - \mu_3\mu_6^2 > 0,$$

$$\begin{aligned}R_{\text{th}_4} = {} & -\mu_2^2 - \mu_3\,\mu_4^2 + \mu_2\,\mu_4\,\mu_5 + 2\mu_2\,\mu_3\,\mu_6 - \mu_1\,\mu_4\,\mu_6 \\ & + \mu_3\,\mu_4\,\mu_5\,\mu_6 - \mu_2\,\mu_6\,\mu_5^2 - (\mu_3\mu_6)^2 + \mu_1\,\mu_5\,\mu_6^2 > 0\end{aligned}$$

$$\begin{aligned}R_{\text{th}_5} = {} & -\mu_2^3 - \mu_2\,\mu_3\,\mu_4^2 + \mu_1\,\mu_4^3 + \mu_4\,\mu_5\,\mu_2^2 \\ & + 2\,\mu_3\,\mu_6\,\mu_2^2 - 3\,\mu_1\,\mu_2\,\mu_4\,\mu_6 \\ & + \mu_2\,\mu_3\,\mu_4\,\mu_5\,\mu_6 - \mu_1\,\mu_4^2\,\mu_5\,\mu_6 - (\mu_2\,\mu_5)^2\,\mu_6 - \mu_2(\mu_3\,\mu_6)^2 \\ & + \mu_1\,\mu_3\,\mu_4\,\mu_6^2 + 2\,\mu_1\,\mu_2\,\mu_5\,\mu_6^2 - \mu_1^2\,\mu_6^3 > 0\end{aligned}$$

$$\begin{aligned}R_{\text{th}_6} = {} & [-\mu_2^3 - \mu_2\,\mu_3\,\mu_4^2 + \mu_1\,\mu_4^3 + \mu_4\,\mu_5\,\mu_2^2 \\ & + 2\,\mu_3\,\mu_6\,\mu_2^2 - 3\,\mu_1\,\mu_2\,\mu_4\,\mu_6 + \mu_2\,\mu_3\,\mu_4\,\mu_5\,\mu_6 \\ & - \mu_1\,\mu_4^2\,\mu_5\,\mu_6 - (\mu_2\,\mu_5)^2\,\mu_6 - \mu_2(\mu_3\,\mu_6)^2 \\ & + \mu_1\,\mu_3\,\mu_4\,\mu_6^2 + 2\,\mu_1\,\mu_2\,\mu_5\,\mu_6^2 - \mu_1^2\,\mu_6^3]\mu_1 \\ = {} & R_{\text{th}_5}\mu_1 > 0.\end{aligned}$$

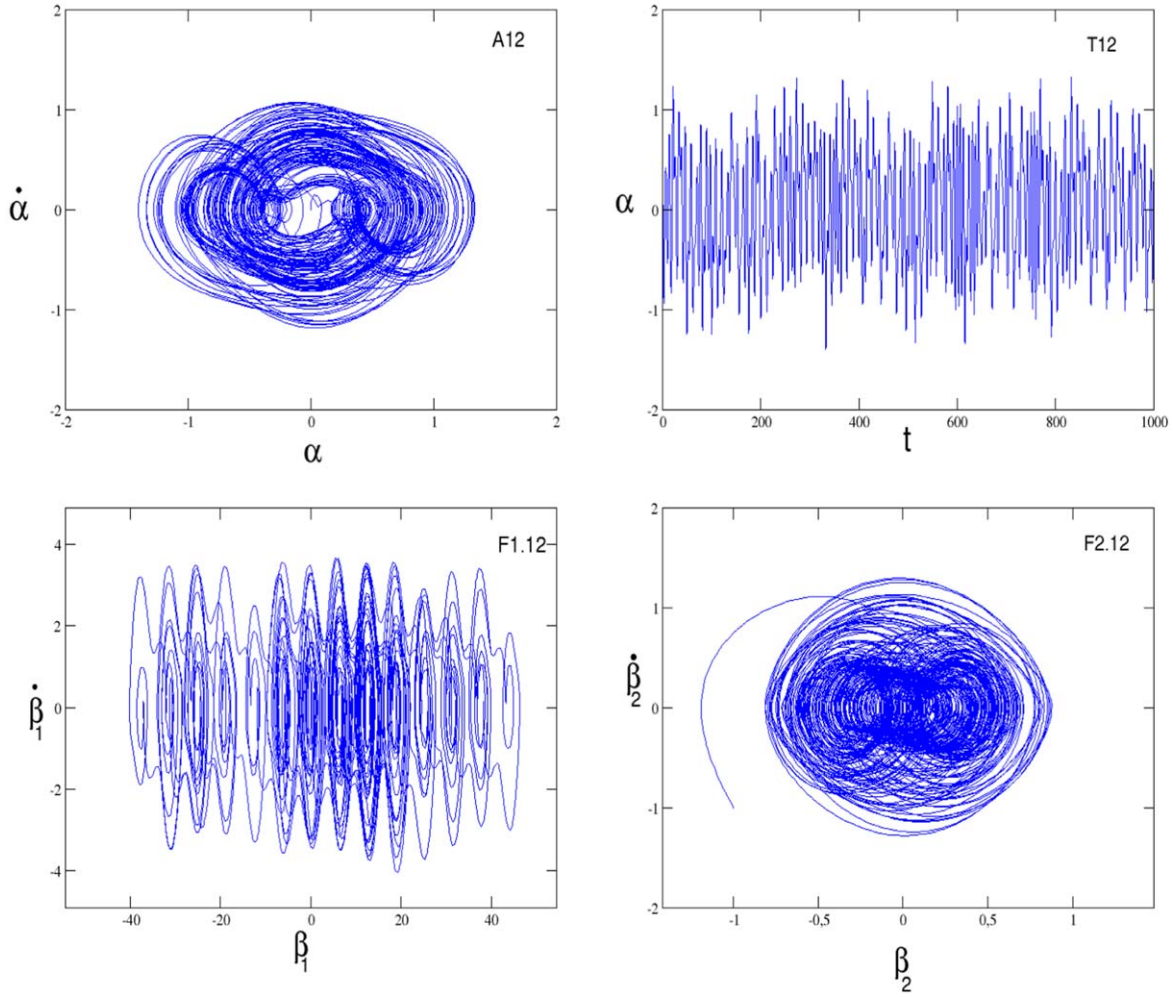

Figure 8. A_{12}: phase space of the flexural vibration of the micro-beam; T_{12}: time histories of the oscillations of the micro-beam; $F1_{12}$: phase difference phase space of the first Josephson junction; $F2_{12}$: phase difference phase space of the second Josephson junction; $\omega_0 = 1$; $i_{G_0} = 2$; $J_1 = 1$; $J_2 = 3$; $J_3 = -1.6$; $J_4 = 2$; $\varphi_{0_1} = 1$; $\varphi_{0_2} = 1.7$; $\sigma_1 = 1$; $\sigma_2 = 2$; $\sigma_3 = 1$; $\sigma_4 = 2$; $\varepsilon_1 = 1.5$; $\varepsilon_2 = 0.9$; $\varepsilon_3 = 0.5$.

In order to verify the stability of our fixed points, we have chosen for the parameters of our junctions some values already existing in the literature that we will exploit. Indeed, the theoretical analysis of stability will be done with the parameters defined as follows: $J_1 = 0.25; J_2 = 0.39; J_3 = 0.26; J_4 = 10^{-4}$; $\varphi_{0_1} = \frac{2\pi}{3}$; $\varphi_{0_2} = \frac{\pi}{6}$; $\sigma_1 = 0.26$; $\sigma_2 = 0.38$; $\sigma_3 = 0.24$; $\sigma_4 = 10^{-4}$; $\varepsilon_1 = 10^{-2}$; $\varepsilon_2 = 1$; $\varepsilon_3 = 0.22$ (see [10, 28, 30]). With these values, we have calculated for the different possible values of $\cos(k_1\pi)$ and $\cos(k_2\pi)$, the coefficients μ_i of the polynomial $P(\kappa)$ and the determinants R_{th_i} of Routh–Hurwitz matrices. The results are shown below:

✓For $k_1 = 2n$, $k_2 = 2n+1$ or $k_1 = 2n+1$, $k_2 = 2n$; $n \in Z$ we have:

$$E^*(\alpha^*, x^*, \beta_1^*, y^*, \beta_2^*, z^*) = \left(0, 0, \frac{2n\pi}{\varphi_{0_1}}, 0, \frac{(2n+1)\pi}{\varphi_{0_2}}, 0\right)$$

or

$$E^*(\alpha^*, x^*, \beta_1^*, y^*, \beta_2^*, z^*) = \left(0, 0, \frac{(2n+1)\pi}{\varphi_{0_1}}, 0, \frac{(2n)\pi}{\varphi_{0_2}}, 0\right); \quad n \in Z.$$

For these values of k_1 and k_2, one can easily see that R_{th_6} and R_{th_5} have opposite signs because $\mu_1 < 0$. The associated fixed points are then unstable.

✓For $k_1 = 2n+1$, $k_2 = 2n+1$; $n \in Z$ we have:

$$E^*(\alpha^*, x^*, \beta_1^*, y^*, \beta_2^*, z^*) = \left(0, 0, \frac{(2n+1)\pi}{\varphi_{0_1}}, 0, \frac{(2n+1)\pi}{\varphi_{0_2}}, 0\right)$$

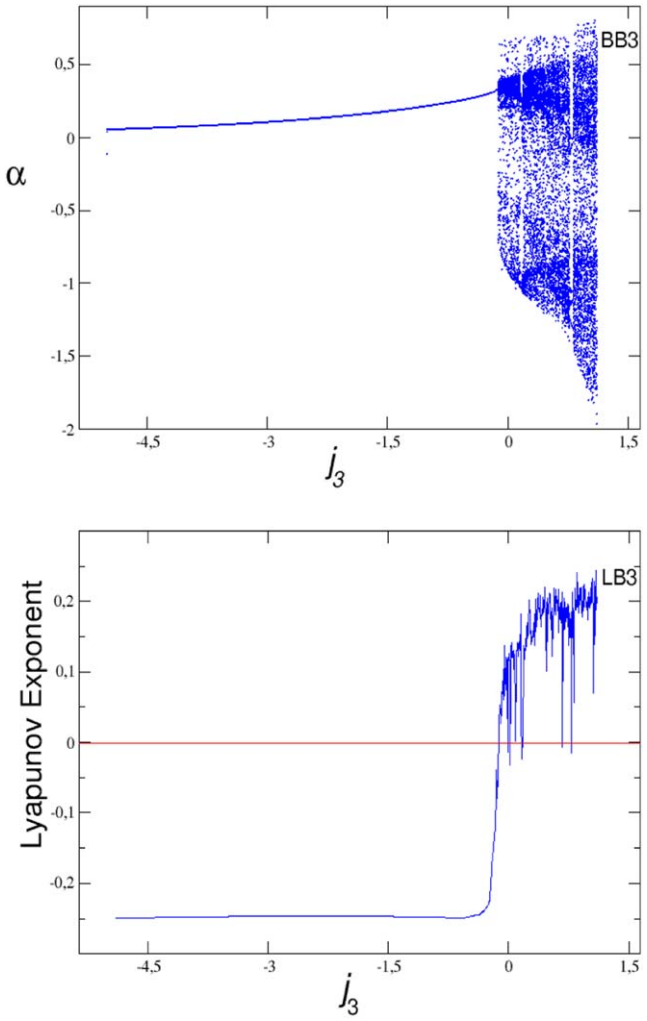

Figure 9. BF2: bifurcation diagram; LF2: Lyapunov exponent; $\omega_0 = 1$; $i_{G_0} = 2$; $J_1 = 1$; $J_2 = 3$; $J_4 = 2$; $\varphi_{0_1} = 1$; $\varphi_{0_2} = 0.5$; $\sigma_1 = 1$; $\sigma_2 = 2$; $\sigma_3 = 1$; $\sigma_4 = 2$; $\varepsilon_1 = 1.5$; $\varepsilon_2 = 0.9$; $\varepsilon_3 = 0.5$.

and

$$\mu_1 = 0.162\,519\,486\,849\,106\,72;$$
$$\mu_2 = -0.260\,488\,343\,322\,645\,37;$$
$$\mu_3 = -0.853\,264\,690\,855\,859\,43;$$
$$\mu_4 = 0.237\,754\,521\,151\,410\,66;$$
$$\mu_5 = -8.139\,215\,245\,249\,7424 \times 10^{-3};$$
$$\mu_6 = 0.519\,999\,990\,239\,739\,42.$$

The Routh–Hurwitz matrices determinants can be written:

$$R_{\text{th}_1} = 0.519\,999\,990\,239\,739\,42;$$
$$R_{\text{th}_2} = -0.241\,986\,912\,999\,499\,68;$$
$$R_{\text{th}_3} = 3.773\,534\,513\,576\,9732 \times 10^{-2};$$
$$R_{\text{th}_4} = -4.411\,646\,090\,376\,4199 \times 10^{-3};$$
$$R_{\text{th}_5} = 1.304\,354\,718\,070\,1526 \times 10^{-3};$$
$$R_{\text{th}_6} = 2.119\,830\,594\,499\,7338 \times 10^{-4}.$$

We then see also that the stability conditions of Routh–Hurwitz are not verified. Indeed, $R_{\text{th}_2} < 0$ and $R_{\text{th}_4} < 0$. The corresponding fixed points are then unstable.

✓For $k_1 = k_2 = 2n$, $n \in Z$ we have:

$$E^*(\alpha^*, x^*, \beta_1^*, y^*, \beta_2^*, z^*) = \left(0, 0, \frac{2n\pi}{\varphi_{0_1}}, 0, \frac{2n\pi}{\varphi_{0_2}}, 0\right);$$

$$\mu_1 = 0.162\,519\,486\,849\,107\,94;$$
$$\mu_2 = 0.263\,738\,732\,986\,976\,59;$$
$$\mu_3 = 1.183\,503\,667\,152\,8403;$$
$$\mu_4 = 0.782\,297\,229\,416\,345\,16;$$
$$\mu_5 = 2.023\,424\,025\,694\,9905;$$
$$\mu_6 = 0.519\,999\,990\,239\,739\,42$$

and the Routh–Hurwitz matrices determinants are:

$$R_{\text{th}_1} = 0.519\,999\,990\,239\,739\,42;$$
$$R_{\text{th}_2} = 0.269\,883\,244\,195\,904\,15;$$
$$R_{\text{th}_3} = 2.825\,367\,319\,464\,7999 \times 10^{-2};$$
$$R_{\text{th}_4} = 4.974\,045\,340\,301\,8942 \times 10^{-3};$$
$$R_{\text{th}_5} = 2.121\,552\,284\,912\,6617 \times 10^{-5};$$
$$R_{\text{th}_6} = 3.447\,935\,886\,664\,3453 \times 10^{-6}.$$

We find that for $k_1 = k_2 = 2n$; $n \in Z$, all fixed points are stable. Indeed, all the determinants of the matrices of Routh–Hurwitz are strictly positive. For $n = 0$, the origin point $E^* = (0, 0, 0, 0, 0, 0)$ is stable as shown in figures 2 and 3. We thus arrive at the end of the analytical studies of the dynamic system. We can retain from this analytical study that for this dynamic system, we have an infinity of fixed points whose stability depends on the conditions of Routh–Hurwitz defined above. For a well-chosen example, we have shown that fixed points $E^* = \left(0, 0, \frac{(2n)\pi}{\varphi_{0_1}}, 0, \frac{(2n)\pi}{\varphi_{0_2}}, 0\right)$, $n \in Z$ are stable. These theoretical results will be checked in the section of the numerical studies (4) where the electrical and dynamic behaviors of the micro-system are simulated for the same values of the parameters.

4. Numerical study and analysis of the effect of the parameters

The aim of this section is to solve numerically, using the order four Runge–Kutta the dynamics equations (14)–(16) to seek the various dynamics of the MEMS. Thus, for the values of the control parameters defined as above, we have plotted the phase diagrams of the micro-beam and of each of the Josephson junctions, then the time histories of the transversal oscillations of the micro-beam; the pulse ω_0 and the amplitude i_{G_0} of the excitation current of the system are chosen equal to 6×10^{-1} and 8×10^{-2} respectively as in [10, 28–30]. Figure 3 illustrates the electrodynamic behavior obtained for the micro-system. We find that the phase spaces of the Josephson junctions (figure 3 P1 and P2) show attractors that reach their limit cycle more quickly while the phase spaces (figure 3 A00″) of the micro-beam show that the oscillations of the micro-beam take a little more time before becoming periodic. The time histories diagram (figure 3 T00″) illustrates this phenomenon. Nevertheless it should be noted that the

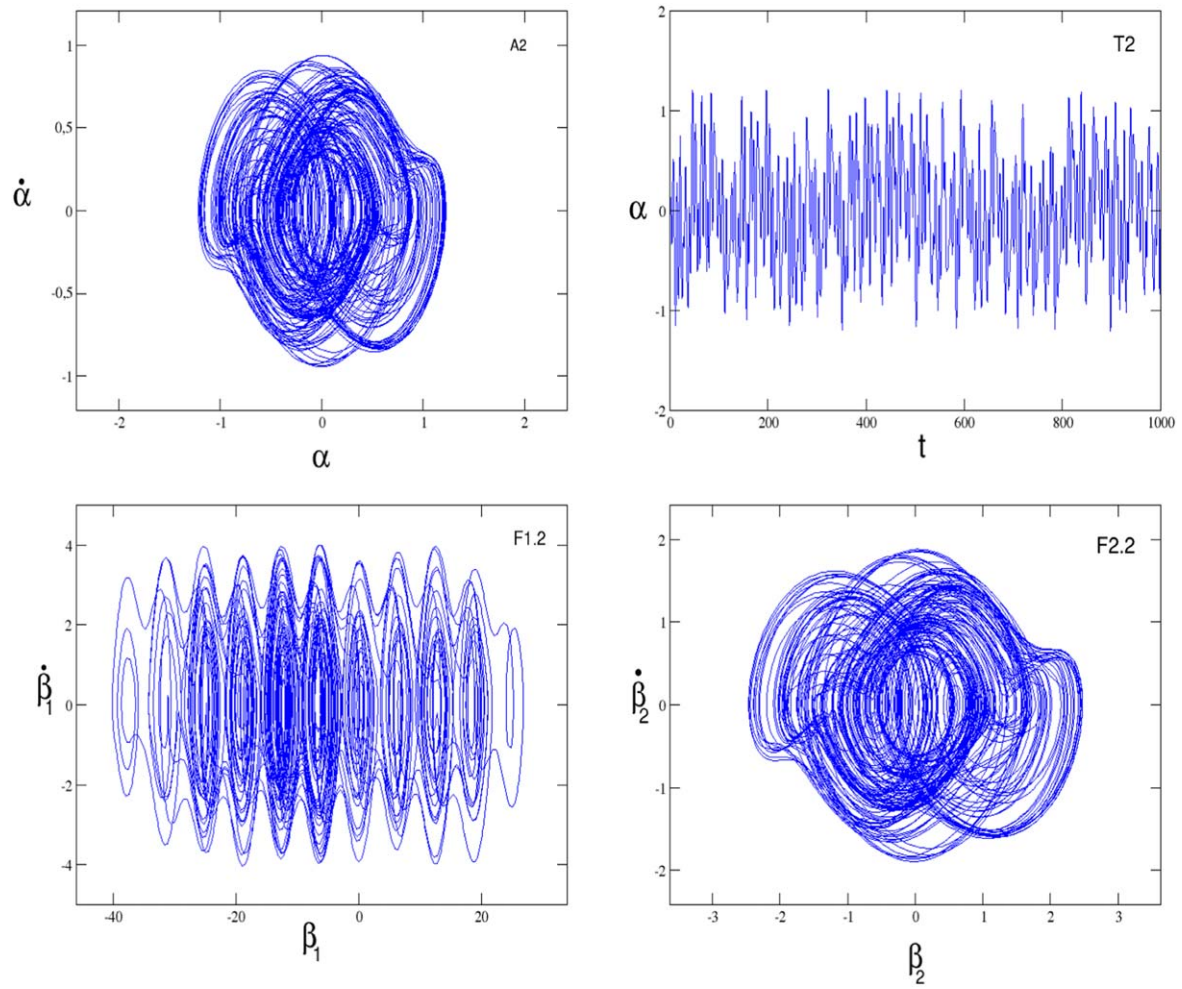

Figure 10. A_2: phase space of the flexural vibration of the micro-beam; T_2: time histories of the oscillations of the micro-beam; $F1_2$: phase difference phase space of the first Josephson junction; $F2_2$: phase difference phase space of the second Josephson junction; $\omega_0 = 1$; $i_{G_0} = 2$; $J_1 = 1$; $J_2 = 3$; $J_3 = 0.34$; $J_4 = 2$; $\varphi_{0_1} = 1$; $\varphi_{0_2} = 0.5$; $\sigma_1 = 1$; $\sigma_2 = 2$; $\sigma_3 = 1$; $\sigma_4 = 2$; $\varepsilon_1 = 1.5$; $\varepsilon_2 = 0.9$; $\varepsilon_3 = 0.5$.

limit cycle is reached quickly and oscillations of the micro-beam become periodic. When ignoring start noise, the diagrams in the figure 3 take the form of the figure 4. These diagrams confirm the origin as the fixed point of the electrodynamic system as provided by the analytical analyzes. We can also hypothesize that Josephson junctions forced the micro-beam to return to their oscillatory dynamic mode.

Now, the goal is to prove the existence or the possibility of having chaotic regimes with at least one of the control parameters of the studied system. To achieve this, we chose to use the i_{G_0} excitation current for two basic reasons. The first reason is that i_{G_0} is the control parameter of the electrodynamic system whose modeling is the easiest. Yamapi and Filatrella in [20] have shown for a system consisting of Josephson junction and an electric resonator that the attractor characterized by a frequency locked to the resonator is most stable for low bias current, when the power dissipated in the cavity is small. Indeed, to check if this results is in agreement with the results of our researches is the second motivation of this choice. Note that the limit cycle of the figure 4 was actually obtained for a small value of the excitation current ($i_{G_0} = 8 \times 10^{-2}$). By varying i_{G_0} from 8×10^{-2} to 5×10^{-1}, we notice that the MEMS has a chaotic behavior (see figure 5).

As expected, the increase in the amplitude of the excitation current considerably changes the oscillatory dynamics of the system. We go from periodic modes to chaotic modes at all levels. This is well justified by the nature of the time histories diagram (see figure 5(p)) which illustrates a completely aperiodic behavior of the mechanical resonator. From before, it can be recalled that the system under study has many chaotic behaviors that can be modulated by means of the excitation current. This result is in perfect conformity with that found by Yamapi and Filatrella in [20] for an electric resonator. The next step in our work is to evaluate the influence of each control parameter on our electro-dynamic system and to bring out the relationship between this parameter and the constituents of our MEMS. Thus, in order to check the rich dynamics of the MEMS, we plot the bifurcation diagram and its corresponding Lyapunov exponents, phase portraits and time histories. We analyze the effects of each parameters of MEMS in the following subsections.

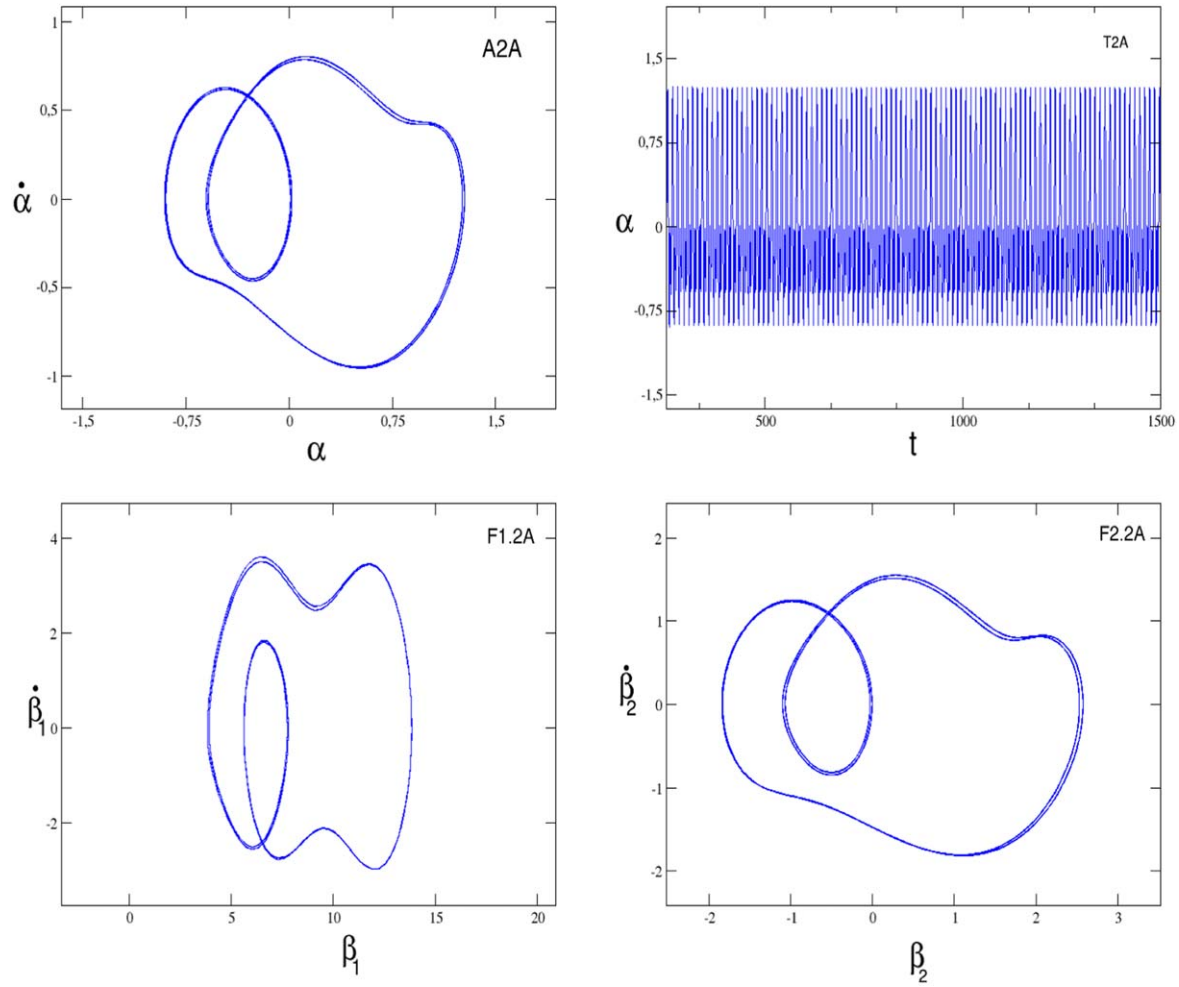

Figure 11. A.2A: phase space of the flexural vibration of the micro-beam; T.2A: time histories of the oscillations of the micro-beam; F1.2A: phase difference phase space of the first Josephson junction; F2.2A: phase difference phase space of the second Josephson junction; $\omega_0 = 1$; $i_{G_0} = 2$; $j_1 = 1$; $j_2 = 3$; $j_3 = 0.48$; $j_4 = 2$; $\varphi_{0_1} = 1$; $\varphi_{0_2} = -3.494$; $\sigma_1 = 1$; $\sigma_2 = 2$; $\sigma_3 = 1$; $\sigma_4 = 2$; $\varepsilon_1 = 1.5$; $\varepsilon_2 = 0.9$;$\varepsilon_3 = 0.5$.

4.1. Influence of the parameter φ_{0_2}

We find the effect of parameter φ_{0_2} on the dynamic of system. Figure 6 shows the bifurcation diagram and the Lyapunov exponents for this parameter where the other parameters are fixed. As it can been seen, the micro-beam can present the periodic, quasi-periodic and chaotic behaviors when the initial phase of second Josephson junction varied.

For appropriate values of φ_{0_2} choice in each domain of figure 6, we plot in figures 7 and 8 the phase portrait and time histories of MEMS. It noted that for $\varphi_{0_2} = -3.494$ the MEMS has the quasi-periodic oscillations (see figure 7) while the chaotic behavior is observed for $\varphi_{0_2} = 1$ (see figure 8). We can conclude that dynamic of MEMS is influenced by the initial phase of second Josephson junction and it is observed a similarity between the two Josephson junctions and the micro-beam.

4.2. Influence of the parameter j_3

In this subsection, we use j_3 as a bifurcation parameter and we plot in figure 9 the bifurcation diagram and its corresponding Lyapunov exponents.

For $-4.5 < j_3 < -0.3$ the micro-beam vibrates periodically with period $1T$ and when $j_3 > -0.3$, we have the chaotic vibrations generally. These different influences of j_3 on the dynamics of the micro-beam once again show the influence of a damping coefficient of second Josephson junction on the latter. The figure 10 illustrates the chaotic vibration of the MEMS for $j_3 = 0.34$. It can be seen from the graphs in figure 10 that any chaotic behavior of the phase difference of one of the Josephson junctions has the same effect on the dynamics of the micro-beam. It is the same for the regular behaviors (see figures 11 and 12). Thus, it can be noted that the junction system confers or imposes its dynamic on the micro-beam. Moreover, there is a degeneracy of the limit cycle when j_3 believes. In fact, for $j_3 < -0.3$ we have a mono-periodic limit cycle but for $j_3 = 0.48$, a first degeneracy is shown and the period of the limit cycle goes from 1 to 3 (figure 11). For $j_3 = 0.7973$ we notice a second degeneracy and the period of the limit cycle goes from 3 to 5 (figure 12). Note also that the origin is not the fixed point for these values of the chosen parameters (see figure 11 F1.2A and figure 12 F1.2B). This confirms the plurality of fixed points of the system.

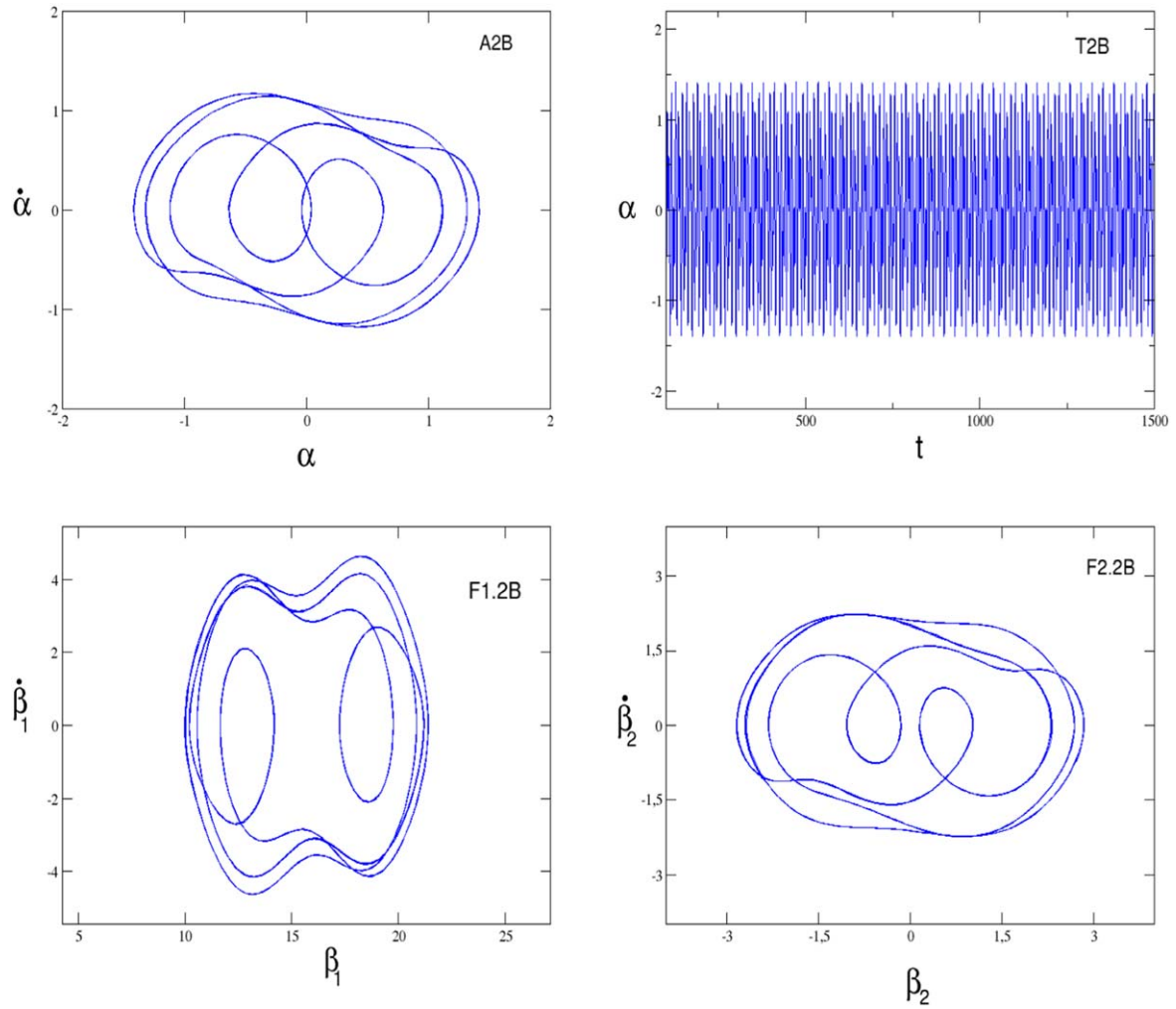

Figure 12. A.2B: phase space of the flexural vibration of the micro-beam; T.2B: time histories of the oscillations of the micro-beam; F1.2B: phase difference phase space of the first Josephson junction; F2.2B: phase difference phase space of the second Josephson junction; $\omega_0 = 1$; $i_{G_0} = 2$; $J_1 = 1$; $J_2 = 3$; $J_3 = 0.7973$; $J_4 = 2$; $\varphi_{0_1} = 1$; $\varphi_{0_2} = -3.494$; $\sigma_1 = 1$; $\sigma_2 = 2$; $\sigma_3 = 1$; $\sigma_4 = 2$; $\varepsilon_1 = 1.5$; $\varepsilon_2 = 0.9$; $\varepsilon_3 = 0.5$.

4.3. Influence of parameter J_4

Using J_4 as the bifurcation parameter, we search the route to chaos of micro-beam and results are plotted in figure 13. It is found that the beam has periodic oscillations for $1 < J_4 < 4.8$ while the beam and the two Josephson junctions have each chaotic oscillations when $J \geqslant 4.8$. For example, figure 14 shows the chaotic motions for $J_4 = 5.54$ and confirm the bifurcation and Lyapunov exponent predictions.

4.4. Influence of the parameter σ_1

The parameter σ_1 is a very important parameter for our system (damping coefficient of the flexural vibration of the micro-beam). Figure 15 represents the bifurcation diagram and its corresponding Lyapunov exponent when σ_1 is varied and other parameters are fixed.

As can been seen, for $1 \leqslant \sigma_1 \leqslant 2.84$, the oscillations are periodic and the associated attractor is monocyclic. For $\sigma_1 \simeq 2.68$, we observe two distinct periods of oscillation with a two periodic attractor. We were particularly interested in the study of this point given the appearance of the bifurcation diagram of the parameter σ_1 at this point. This dynamic is illustrated by figure 16 if $\sigma_1 = 2.68$. When $\sigma_1 \in]2.84; 2.94[$, as predicted by the bifurcation diagram, we obtain a two limit cycles which are shown in figure 17 for $\sigma_1 = 2.89$. The chaotic motions are observed $\sigma_1 \geqslant 2.94$. We can conclude that the damping coefficient of the flexural vibration of the micro-beam affect the MEMS dynamics and the beam and the two Josephson junctions are the same behaviors when σ_1 varied. From what went before it can be concluded that the dynamic of the micro-beam is in agreement with that of Josephson junctions. The dynamics of the entire system can be controlled through one of the elements of the electrical or mechanical part. This shows the ability of this MEMS due to its sensitivity at all levels in the field of physical applications. Since the damping of the vibrating membrane of the micro-beam is also proportional to the speed of the latter, it can be concluded that the whole dynamics of the MEMS can be modeled by the variation of the magnetic force $\vec{F} = i_s \times \vec{B} \wedge \vec{L}$. Indeed, according Newton's second law we

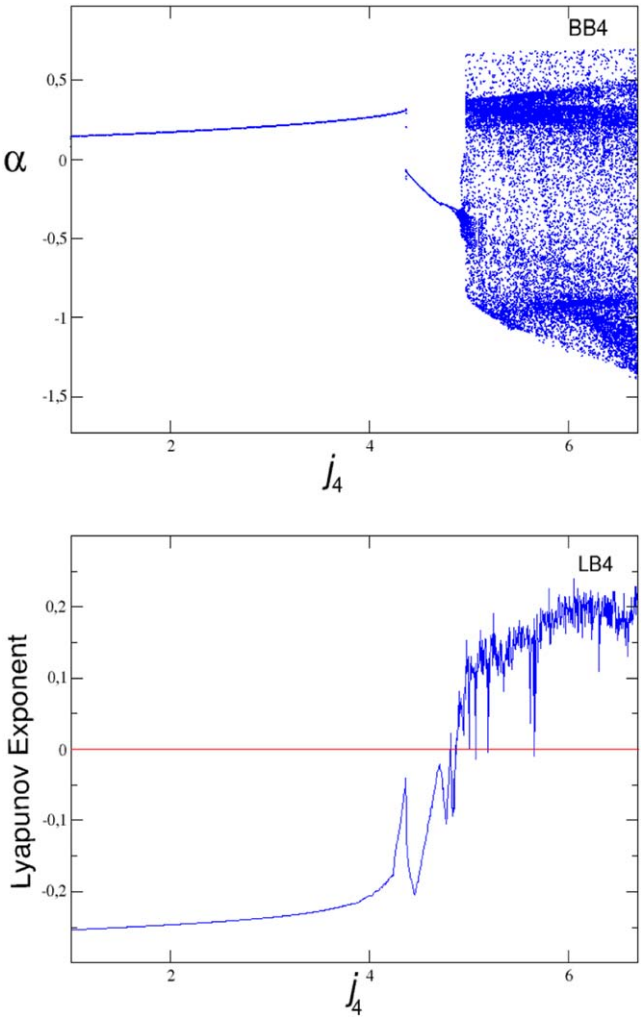

Figure 13. BF2: bifurcation diagram; LF2: Lyapunov exponent; $\omega_0 = 1$; $i_{G_0} = 2$; $J_1 = 1$; $J_2 = 3$; $J_3 = -1.6$; $\varphi_{0_1} = 1$; $\varphi_{0_2} = 0.5$; $\sigma_1 = 1$; $\sigma_2 = 2$; $\sigma_3 = 1$; $\sigma_4 = 2$; $\varepsilon_1 = 1.5$; $\varepsilon_2 = 0.9$; $\varepsilon_3 = 0.5$.

have: $\sum \vec{F}_{\text{ext}} = m\frac{\vec{\text{d}}\dot{\alpha}}{\text{d}t}$. Because the actuating force $\vec{F}$ depends strongly on the intensity of the magnetic field $\vec{B}$, we can conclude that this MEMS according to its electrodynamic modes can not only detect the magnetic fields but also provide information on the characteristics of the magnetic field in which it bathed.

4.5. Influence of the parameter σ_2

The parameter σ_2 coefficient of $\sin(\varphi_{0_2}\beta_2)$ is also an important control parameter of the dynamical system studied. Should we recall, our main objective to study to examine the influence of Josephson junctions on the vibrational modes of a micro-beam. The various dynamics predicted by the bifurcation diagram of figure 18 above confirm the action of the second Josephson junction on the vibratory modes of the micro-beam. Figures 19 and 20 illustrate some of the periodic dynamic behaviors of the MEMS for $\sigma_2 = 5.66$ and $\sigma_2 = 9.09$ respectively. The chaotic mode is confirmed for $\sigma_2 = 8.1$ (see figure 21).

4.6. Influence of the parameters $\sigma_3, \sigma_4, \varepsilon_1$, and ε_3

We then studied the influence of σ_3, σ_4, ε_1, and ε_3 on dynamic of the MEMS. For this purpose, we plot the bifurcation and its corresponding Lyapunov exponents in figures 22, 23, when σ_3 , σ_4 are varied respectively. It noted that the chaotic oscillations appear in small domain while the regular vibrations exist on the rest domain. Figure 24 shows the chaotic vibration for the micro-beam and for the two Josephson junctions when $\sigma_4 = 3.34$ chosen in chaotic domain predict by bifurcation diagram. This confirm the bifurcation and Lyapunov predictions. In figures 25, 26 we plot the bifurcation and its corresponding Lyapunov exponents by using ε_1 and ε_3 as bifurcation parameters. The same observations in the cases of σ_3, σ_4 are made. Figure 27 represents the phase portraits and time histories of the MEMS for $\varepsilon_1 = 1.7$ and confirm the bifurcation and Lyapunov exponents predictions. Although these observations, we noticed that J_4, σ_4, and ε_3 which depend of the magnetic field $\vec{B}$ favor more regular vibrations and therefore can be used to control the chaotic vibrations of the MEMS. In the absence of the magnetic field ($B = 0$), the micro-beam should have a static behavior that is fixed in its equilibrium position. Assuming that the dynamics of the micro-beam influence that of the Josephson junctions, we should note a stability expressed by a periodic oscillation at the junctions under the effect of the generator excitation. This hypothesis has been verified as shown by the numerical results of figure 28. The time histories (figure 28:f) of the flexural vibration is linear. This justifies the absence of oscillation of the vibrating membrane of the micro-beam and its equilibrium state. Figures 28: g and h representing the phase spaces of the junctions illustrate a periodic behavior. We can then confirm that for this MEMS, the micro-beam dynamics and electrical behaviors are in good agreement. It should also be noted that this MEMS can serve as a magnetic field detector and a good high precision actuator.

4.7. Influence of the parameter i_{G_0}

After studying the influence of the internal parameters of the MEMS, it is important to analyze the effects of the external excitation. For this end, we plot the bifurcation diagram and its corresponding Lyapunov exponents when the amplitude i_{G_0} of external voltage varied and other parameter are fixed. The results are presented in figure 29. It observed that the beam has periodic, multi-periodic, quasi-periodic and chaotic vibrations for $i_{G_0} \in [0, 15]$. It also obtained from this figure the intermittency phenomenon. The chaotic vibration obtained is illustrated in figure 30 for $i_{G_0} = 5.45$. The excitation voltage influence highly the MEMS dynamics and can be used to vary the dynamics of the beam according to the wishes of the user.

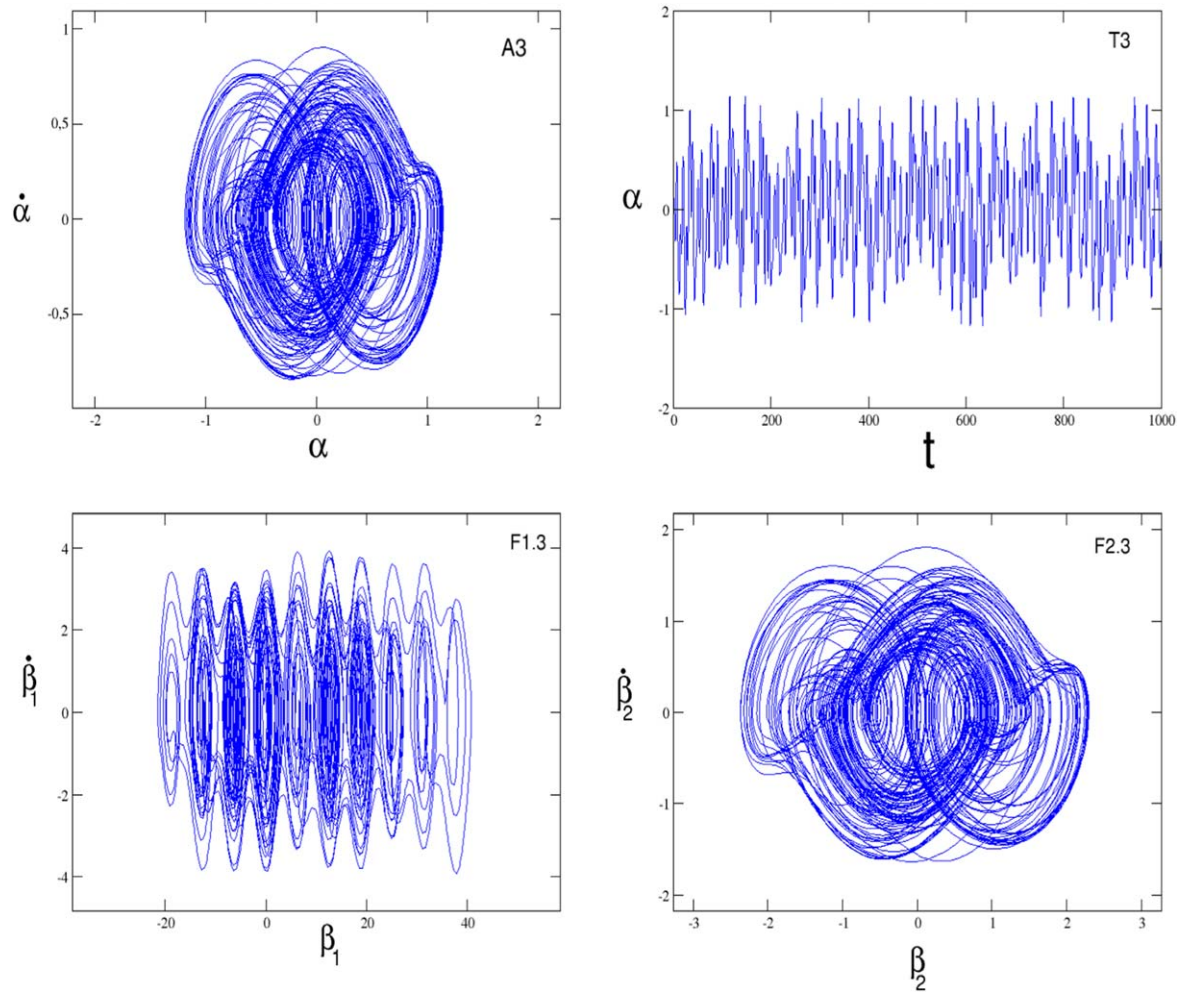

Figure 14. A_3: phase space of the flexural vibration of the micro-beam; T_3: time histories of the oscillations of the micro-beam; F1.3: phase difference phase space of the first Josephson junction; F2.3: phase difference phase space of the second Josephson junction; $\omega_0 = 1$; $i_{G_0} = 2$; $J_1 = 1$; $J_2 = 3$; $J_3 = -1.6$; $J_4 = 5.54$; $\varphi_{0_1} = 1$; $\varphi_{0_2} = 0.5$; $\sigma_1 = 1$; $\sigma_2 = 2$; $\sigma_3 = 1$; $\sigma_4 = 2$; $\varepsilon_1 = 1.5$; $\varepsilon_2 = 0.9$; $\varepsilon_3 = 0.5$.

5. Conclusion

This study focused on a MEMS whose essential components are the Josephson junction and the micro-beam. The main objectives of this study are to analyze the influence of the voltage-frequency converters that are the Josephson junctions on the dynamics of the micro-beam and to evaluate the utility of this type of MEMS. For this dynamic system, an infinite number of fixed points is obtained. For a well chosen example, on the one hand, we have shown that the fixed points are stable when $k = 2n$ and unstable for $k = 2n + 1$. Through the phase spaces on the other hand, we have shown that the dynamic behaviors of the micro-beam are strongly related to those of the two Josephson junctions. The chaotic behavior of one induces that of the micro-beam. The influence of each control parameter has been studied and some dynamics have been illustrated. It goes out of this study also that several chaotic regimes are obtained. Given its proven importance since the 20th century, chaos serves in several scientific fields. The one we have studied here can be used in the field of communication and information on the one hand and in the field of the determination of weak magnetic fields on the other hand. The microscopic size and the convertibility voltage-frequency of this MEMS confers several other interesting potentialities to it. In another work, we intend to render energy autonomous this MEMS in order to find applications in the field of space projects where the economy electrical energy remains an asset for the devices. The main objectives of our next research will be to first build this MEMS in order to find convincing applications and in a second time, extend this study to the nanoscale given the potential, progress and projections given by Roukes in [31] on NEMS (nano-electro-mechanical-systems).

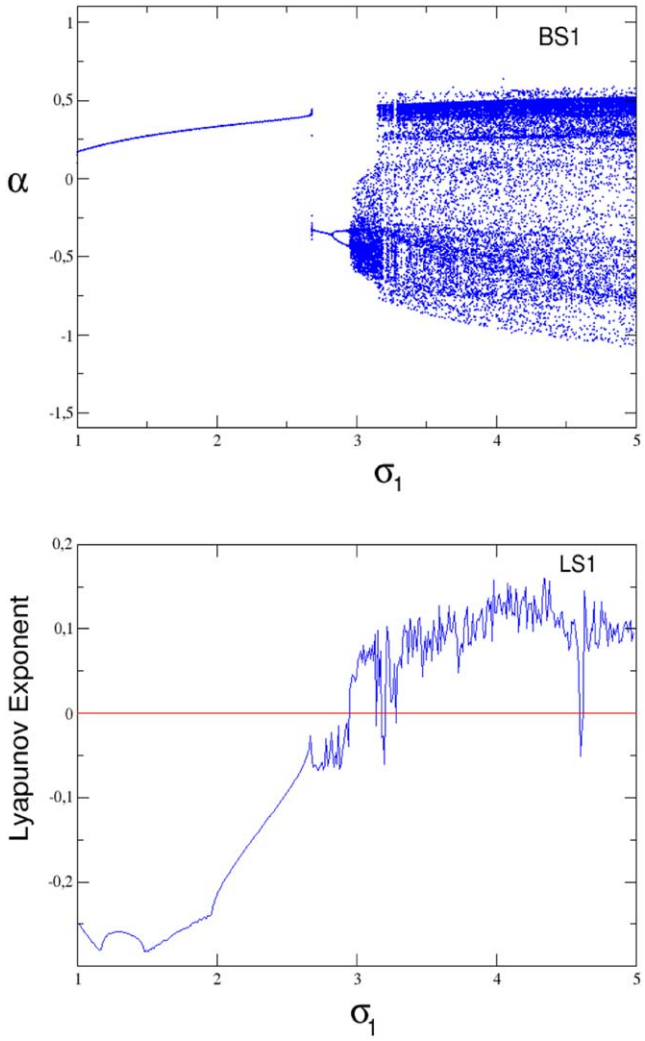

Figure 15. BS1: bifurcation diagram; LS1: Lyapunov exponent: $\omega_0 = 1$; $i_{G_0} = 2$; $J_1 = 1$; $J_2 = 3$; $J_3 = -1.6$; $J_4 = 2$; $\varphi_{0_1} = 1$; $\varphi_{0_2} = 0.5$; $\sigma_1 = 1$; $\sigma_2 = 2$; $\sigma_3 = 1$; $\sigma_4 = 2$; $\varepsilon_1 = 1.5$; $\varepsilon_2 = 0.9$; $\varepsilon_3 = 0.5$.

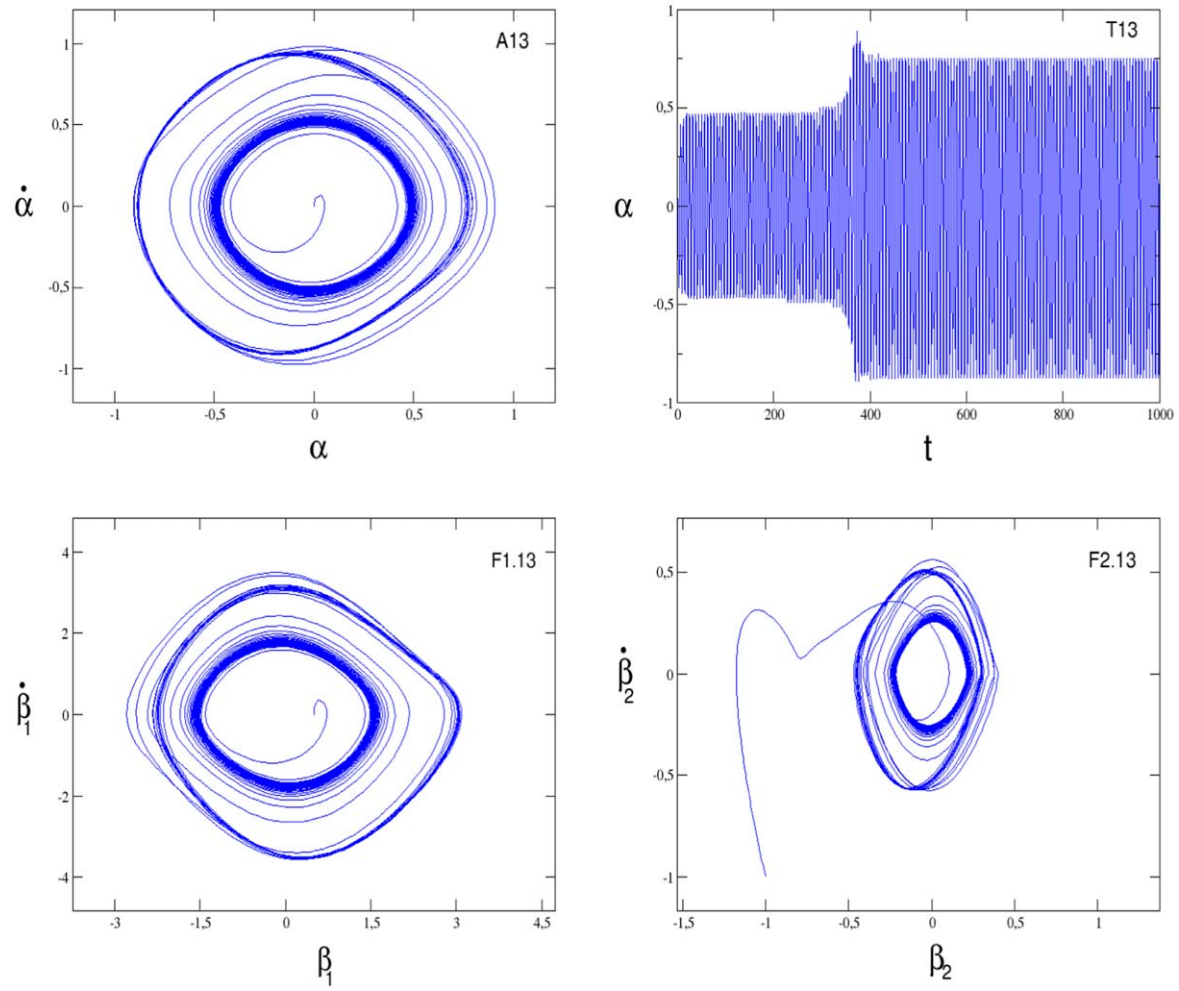

Figure 16. A.13: phase space of the flexural vibration of the micro-beam; T.13: time histories of the oscillations of the micro-beam; F1.13: phase difference phase space of the first Josephson junction; F2.13: phase difference phase space of the second Josephson junction: $\omega_0 = 1$; $i_{G_0} = 2$; $J_1 = 1$; $J_2 = 3$; $J_3 = -1.6$; $J_4 = 2$; $\varphi_{0_1} = 1$; $\varphi_{0_2} = 0.5$; $\sigma_1 = 2.68$; $\sigma_2 = 2$; $\sigma_3 = 1$; $\sigma_4 = 2$; $\varepsilon_1 = 1.5$; $\varepsilon_2 = 0.9$; $\varepsilon_3 = 0.5$.

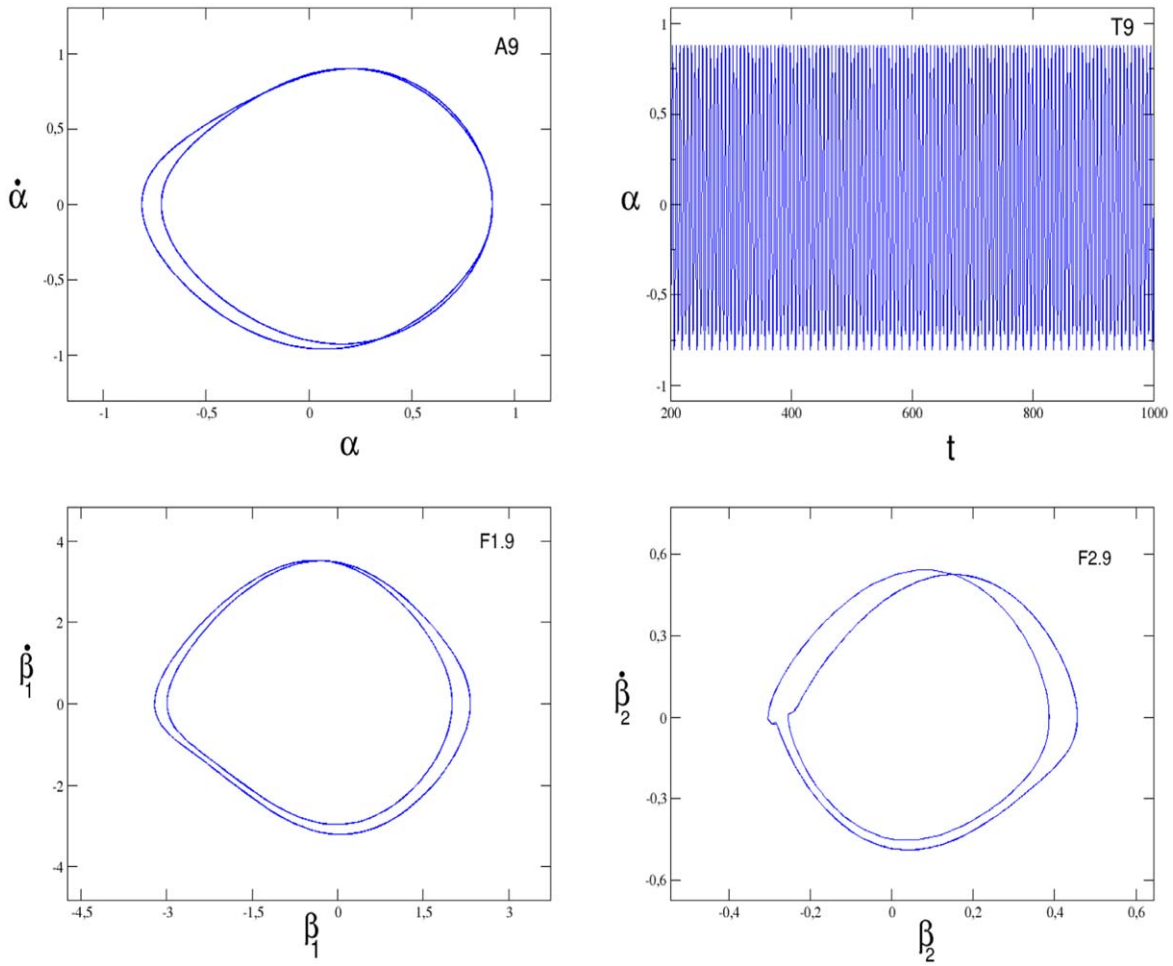

Figure 17. A_9: phase space of the flexural vibration of the micro-beam; T_9: time histories of the oscillations of the micro-beam; $F1_9$: phase difference phase space of the first Josephson junction; $F2_9$: phase difference phase space of the second Josephson junction; $\omega_0 = 1$; $i_{G_0} = 2$; $J_1 = 1$; $J_2 = 3$; $J_3 = -1.6$; $J_4 = 2\varphi_{0_1} = 1$; $\varphi_{0_2} = 0.5$; $\sigma_1 = 2.89$; $\sigma_2 = 2$; $\sigma_3 = 1$; $\sigma_4 = 2$; $\varepsilon_1 = 1.5$; $\varepsilon_2 = 0.9$; $\varepsilon_3 = 0.5$.

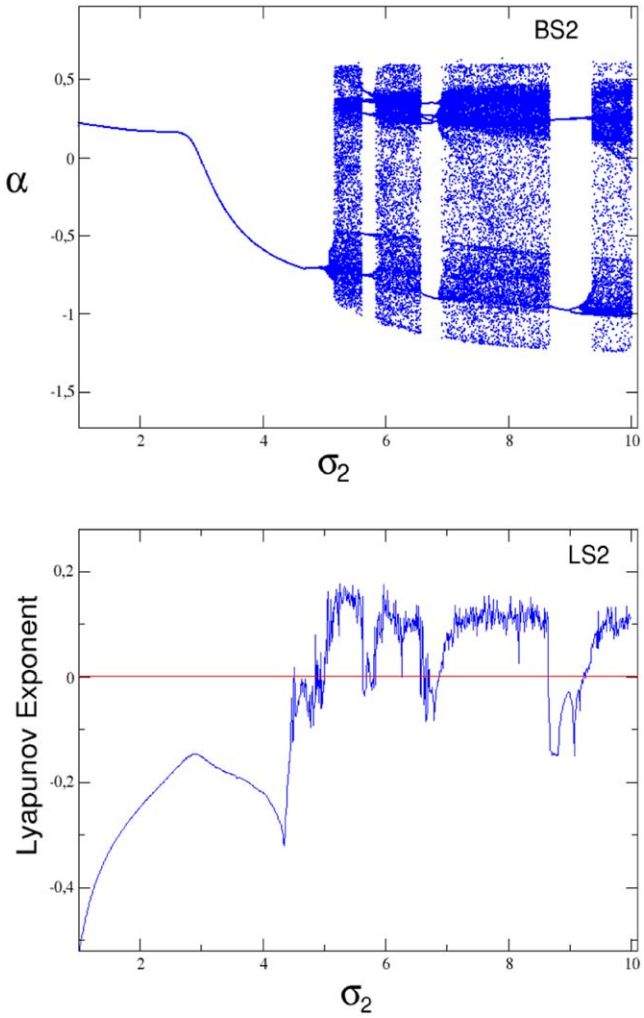

Figure 18. BS2: bifurcation diagram; LS2: Lyapunov exponent; $\omega_0 = 1$; $i_{G_0} = 2$; $J_1 = 1$; $J_2 = 3$; $J_3 = -1.6$; $J_4 = 2$; $\varphi_{0_1} = 1$; $\varphi_{0_2} = 0.5$; $\sigma_1 = 1$; $\sigma_3 = 1$; $\sigma_4 = 2$; $\varepsilon_1 = 1.5$; $\varepsilon_2 = 0.9$; $\varepsilon_3 = 0.5$.

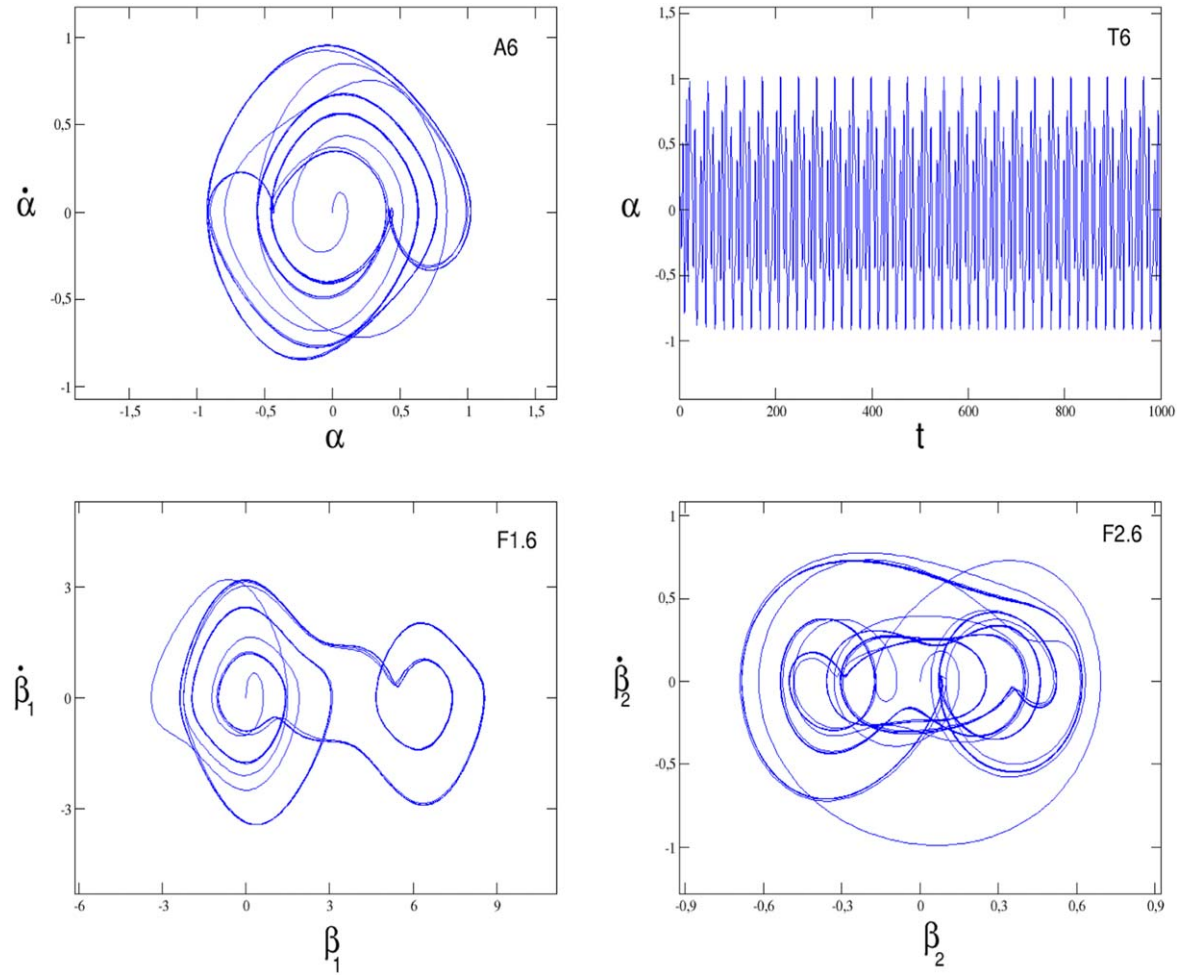

Figure 19. A_6: phase space of the flexural vibration of the micro-beam; T_6: time histories of the oscillations of the micro-beam; $F1_6$: phase difference phase space of the first Josephson junction; $F2_6$: phase difference phase space of the second Josephson junction; $\omega_0 = 1$; $i_{G_0} = 2$; $J_1 = 1$; $J_2 = 3$; $J_3 = -1.6$; $J_4 = 2\varphi_{0_1} = 1$; $\varphi_{0_2} = 0.5$; $\sigma_1 = 1$; $\sigma_2 = 5.66$; $\sigma_3 = 1$; $\sigma_4 = 2$; $\varepsilon_1 = 1.5$; $\varepsilon_2 = 0.9$; $\varepsilon_3 = 0.5$.

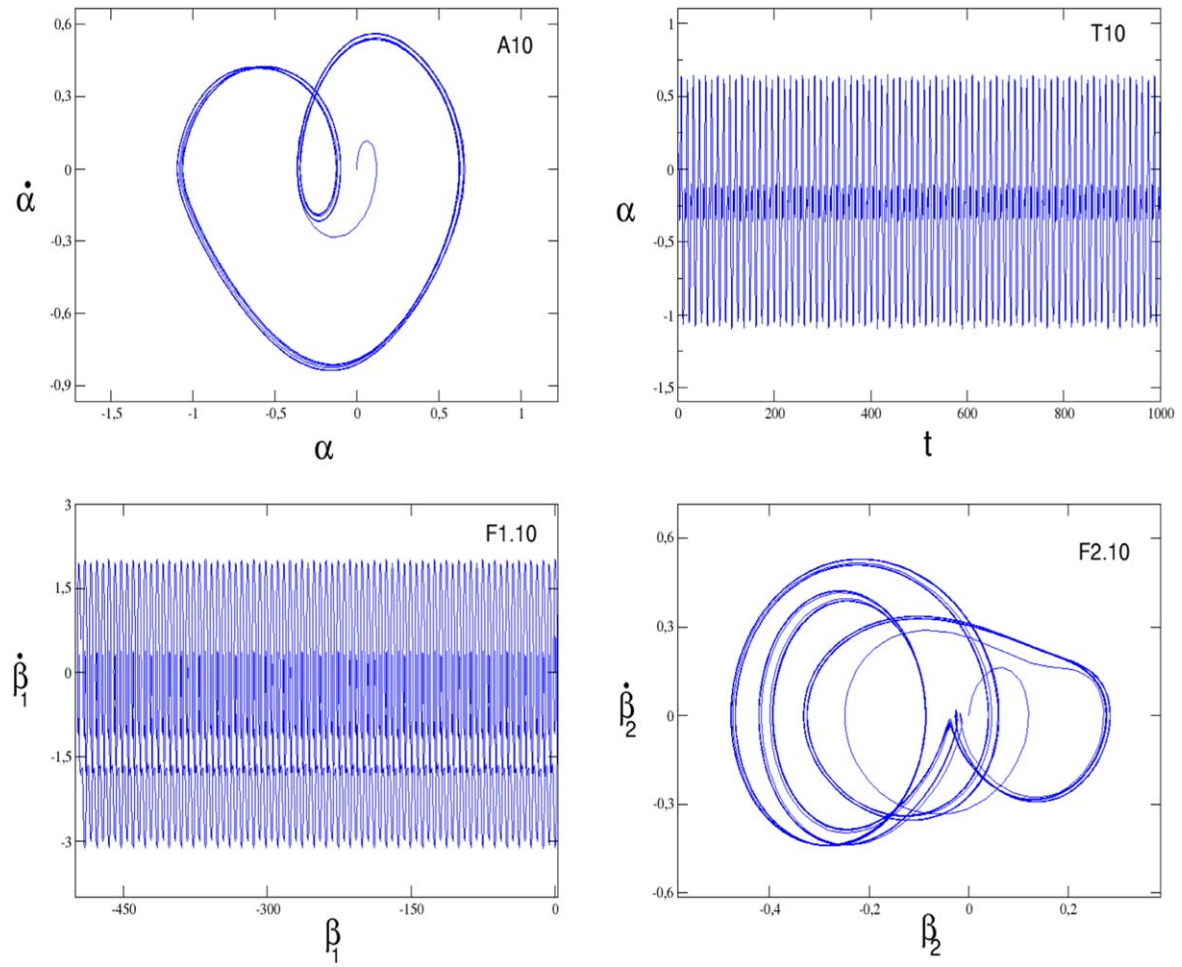

Figure 20. A_{10}: phase space of the flexural vibration of the micro-beam; T_{10}: time histories of the oscillations of the micro-beam; $F1_{10}$: phase difference phase space of the first Josephson junction; $F2_{10}$: phase difference phase space of the second Josephson junction; $\omega_0 = 1$; $i_{G_0} = 2; J_1 = 1; J_2 = 3; J_3 = -1.6; J_4 = 2\varphi_{0_1} = 1; \varphi_{0_2} = 0.5; \sigma_1 = 1; \sigma_2 = 9.09; \sigma_3 = 1; \sigma_4 = 2; \varepsilon_1 = 1.5; \varepsilon_2 = 0.9; \varepsilon_3 = 0.5$.

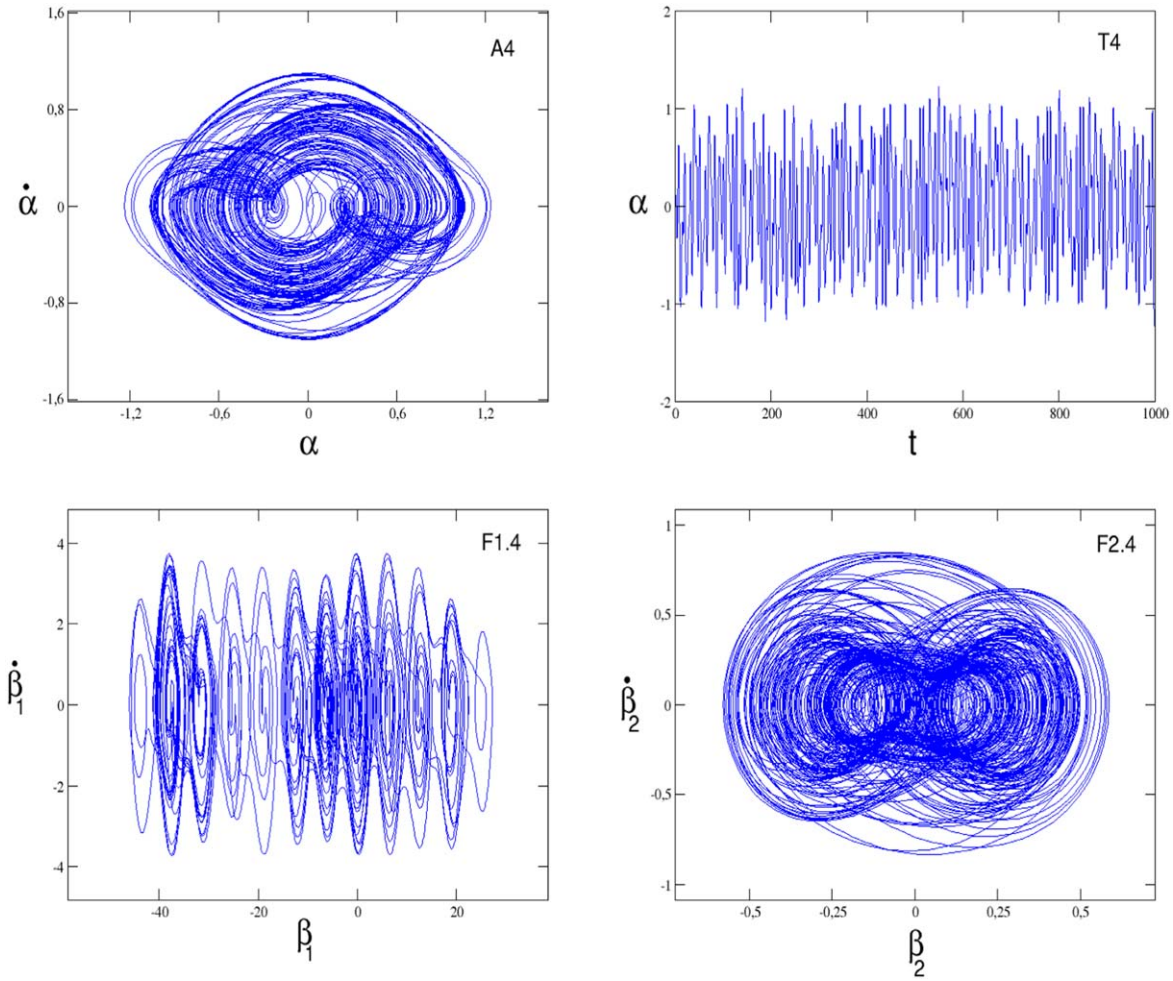

Figure 21. A_4: phase space of the flexural vibration of the micro-beam; T_4: time histories of the oscillations of the micro-beam; $F1_4$: phase difference phase space of the first Josephson junction; $F2_4$: phase difference phase space of the second Josephson junction; $\omega_0 = 1$; $i_{G_0} = 2$; $J_1 = 1$; $J_2 = 3$; $J_3 = -1.6$; $J_4 = 2\varphi_{0_1} = 1$; $\varphi_{0_2} = 0.5$; $\sigma_1 = 1$; $\sigma_2 = 8.1$; $\sigma_3 = 1$; $\sigma_4 = 2$; $\varepsilon_1 = 1.5$; $\varepsilon_2 = 0.9$; $\varepsilon_3 = 0.5$.

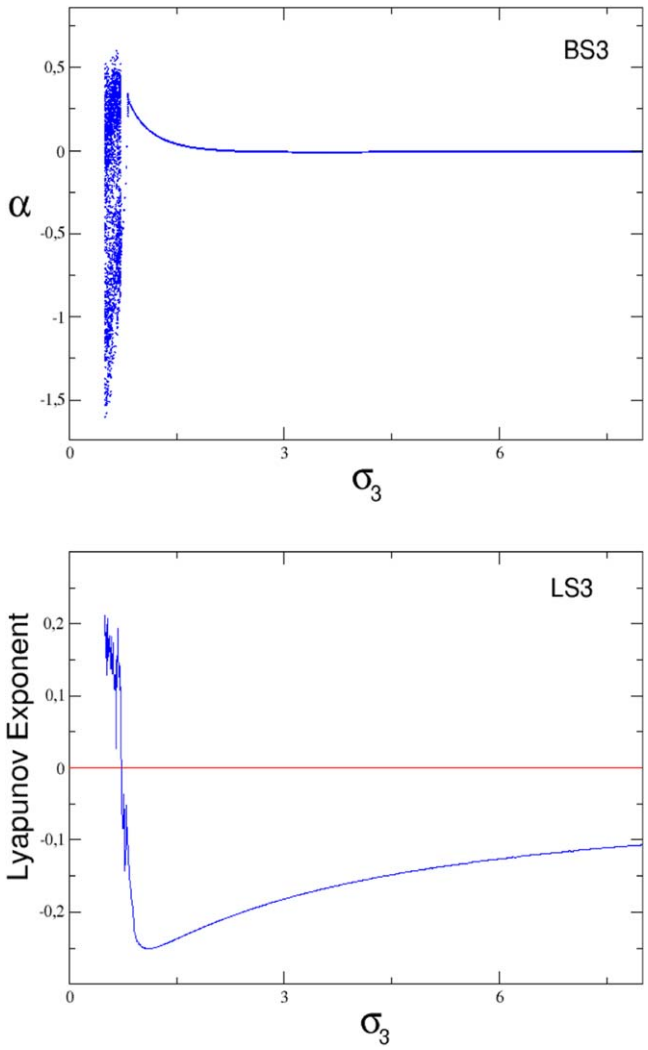

Figure 22. BS3: bifurcation diagram; LS3: Lyapunov exponent; $\omega_0 = 1$; $i_{G_0} = 2$; $J_1 = 1$; $J_2 = 3$; $J_3 = -1.6$; $J_4 = 2$; $\varphi_{0_1} = 1$; $\varphi_{0_2} = 0.5$; $\sigma_1 = 1$; $\sigma_2 = 2$; $\sigma_4 = 2$; $\varepsilon_1 = 1.5$; $\varepsilon_2 = 0.9$; $\varepsilon_3 = 0.5$.

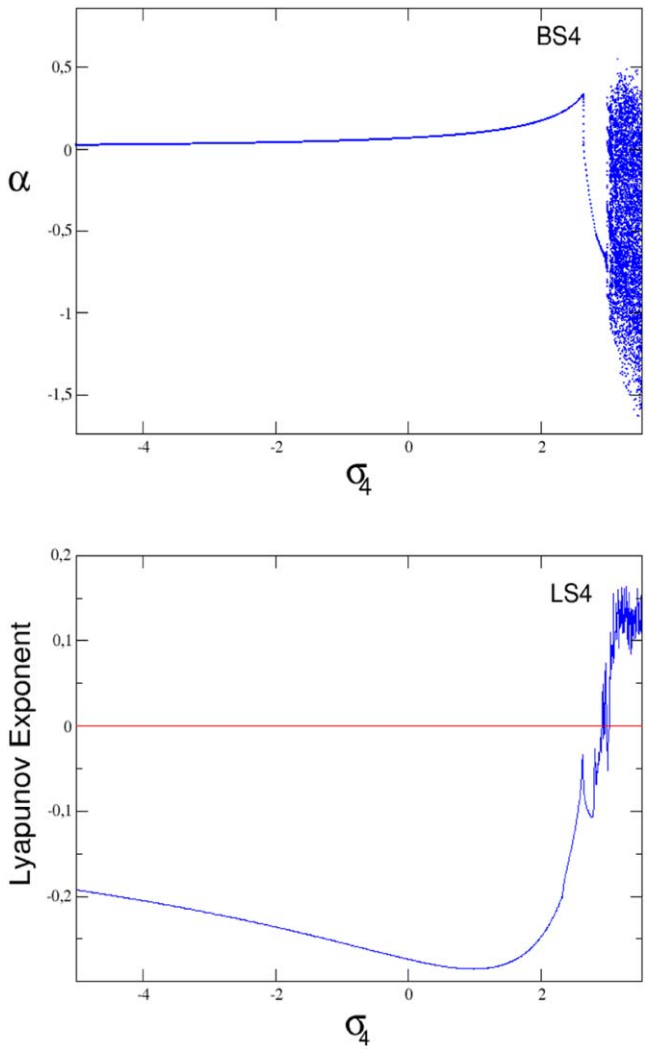

Figure 23. BS4: bifurcation diagram; LS4: Lyapunov exponent; $\omega_0 = 1$; $i_{G_0} = 2$; $J_1 = 1$; $J_2 = 3$; $J_3 = -1.6$; $J_4 = 2$; $\varphi_{0_1} = 1$; $\varphi_{0_2} = 0.5$; $\sigma_1 = 1$; $\sigma_2 = 2$; $\sigma_3 = 1$; $\varepsilon_1 = 1.5$; $\varepsilon_2 = 0.9$; $\varepsilon_3 = 0.5$.

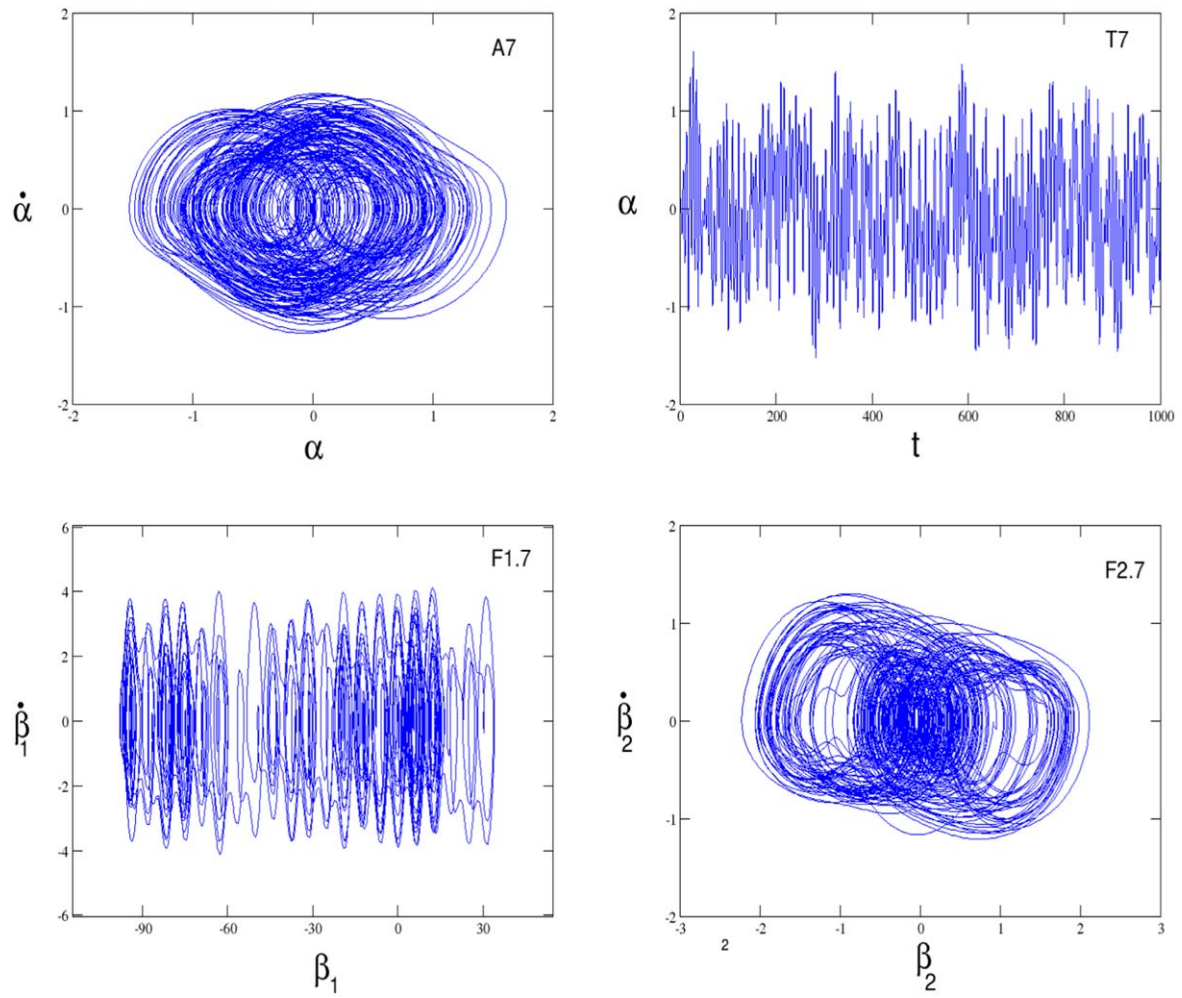

Figure 24. A_7: phase space of the flexural vibration of the micro-beam; T_7: time histories of the oscillations of the micro-beam; $F1_7$: phase difference phase space of the first Josephson junction; $F2_7$: phase difference phase space of the second Josephson junction; $\omega_0 = 1$; $i_{G_0} = 2; J_1 = 1; J_2 = 3; J_3 = -1.6; J_4 = 2\varphi_{0_1} = 1; \varphi_{0_2} = 0.5; \sigma_1 = 1; \sigma_2 = 2; \sigma_3 = 1; \sigma_4 = 3.34; \varepsilon_1 = 1.5; \varepsilon_2 = 0.9; \varepsilon_3 = 0.5$.

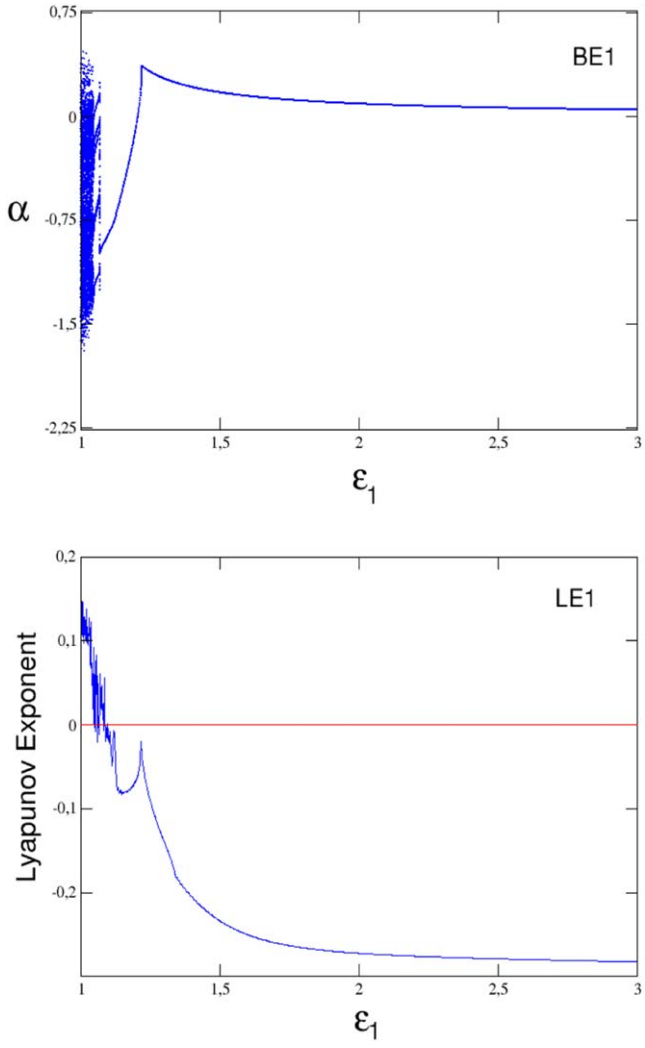

Figure 25. BE1: bifurcation diagram; LE1: Lyapunov exponent; $\omega_0 = 1$; $i_{G_0} = 2$; $J_1 = 1$; $J_2 = 3$; $J_3 = -1.6$; $J_4 = 2$; $\varphi_{0_1} = 1$; $\varphi_{0_2} = 0.5$; $\sigma_1 = 1$; $\sigma_2 = 2$; $\sigma_3 = 1$; $\sigma_4 = 1$; $\varepsilon_2 = 0.9$; $\varepsilon_3 = 0.5$.

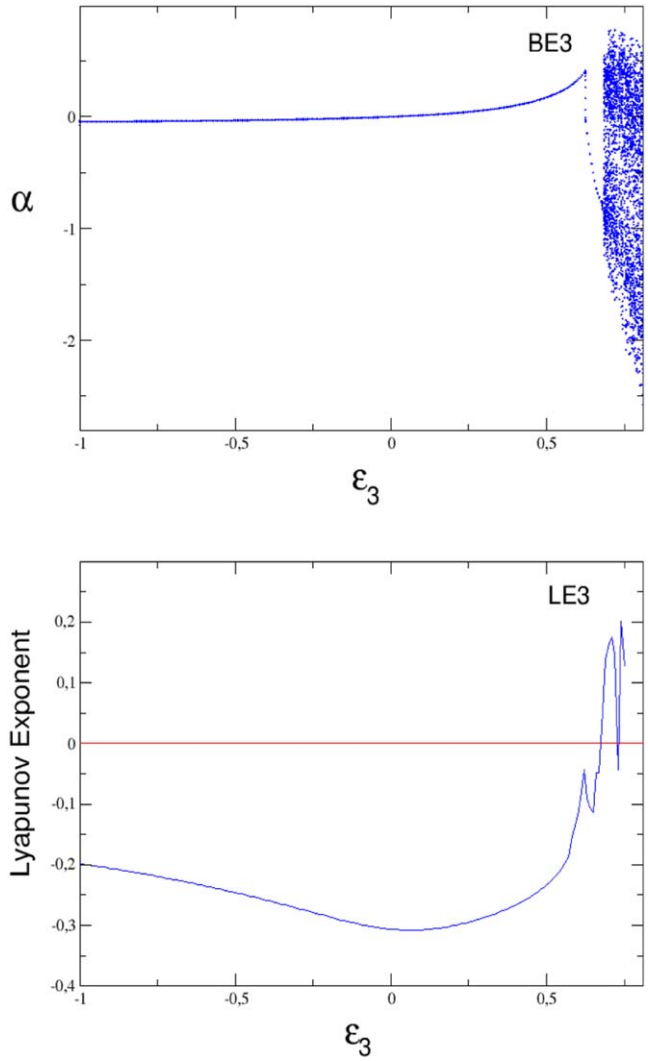

Figure 26. BE3: bifurcation diagram; LE3: Lyapunov exponent; $\omega_0 = 1$; $i_{G_0} = 2$; $J_1 = 1$; $J_2 = 3$; $J_3 = -1.6$; $J_4 = 2$; $\varphi_{0_1} = 1$; $\varphi_{0_2} = 0.5$; $\sigma_1 = 1$; $\sigma_2 = 2$; $\sigma_3 = 1$; $\sigma_4 = 1$; $\varepsilon_1 = 1.5\varepsilon_2 = 0.9$.

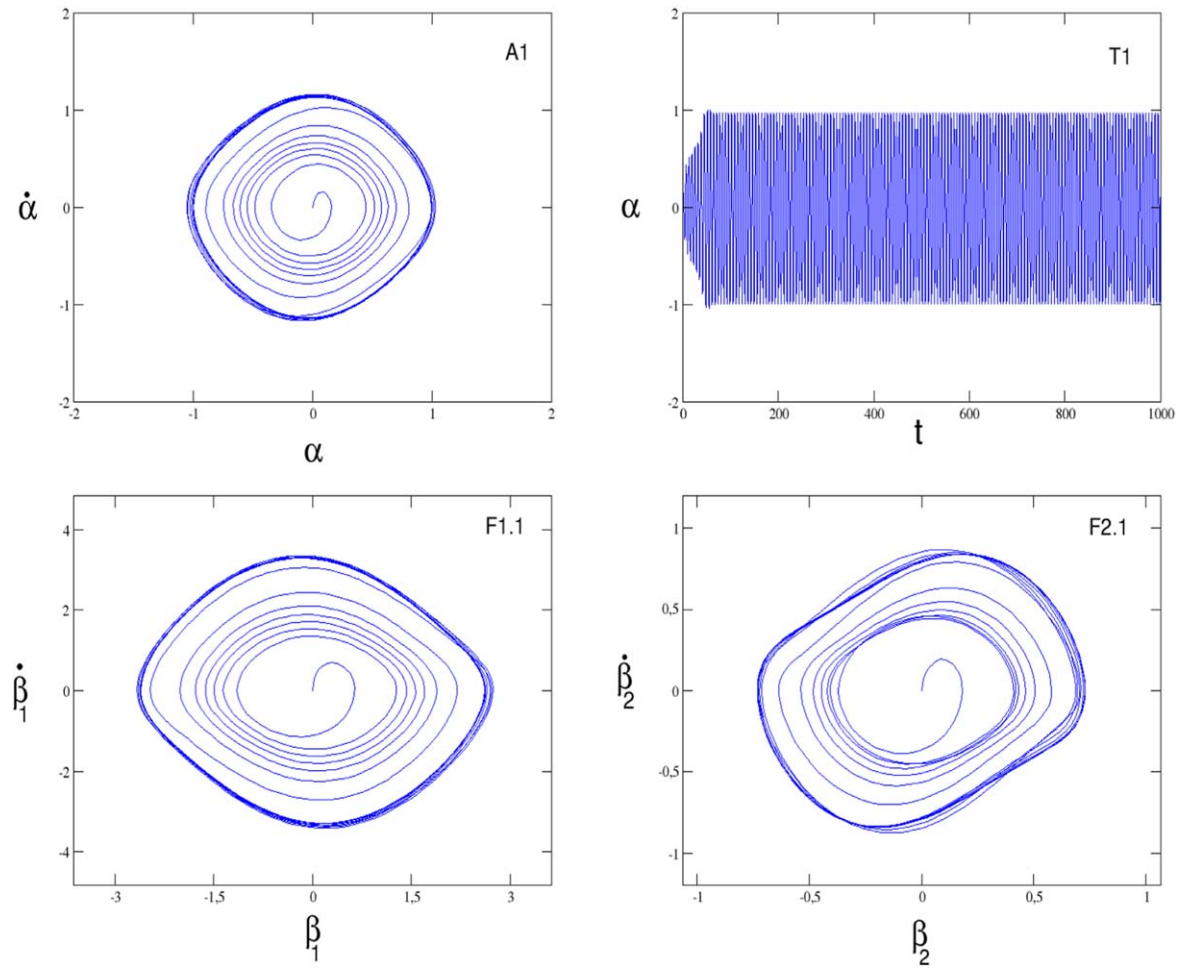

Figure 27. A_1: phase space of the flexural vibration of the micro-beam; T_1: time histories of the oscillations of the micro-beam; $F1_1$: phase difference phase space of the first Josephson junction; $F2_1$: phase difference phase space of the second Josephson junction; $\omega_0 = 1$; $i_{G_0} = 2; J_1 = 1; J_2 = 3; J_3 = -1.6; J_4 = 2\varphi_{0_1} = 1; \varphi_{0_2} = 0.5; \sigma_1 = 1; \sigma_2 = 2; \sigma_3 = 1; \sigma_4 = 2; \varepsilon_1 = 1.7; \varepsilon_2 = 0.9; \varepsilon_3 = 0.5$.

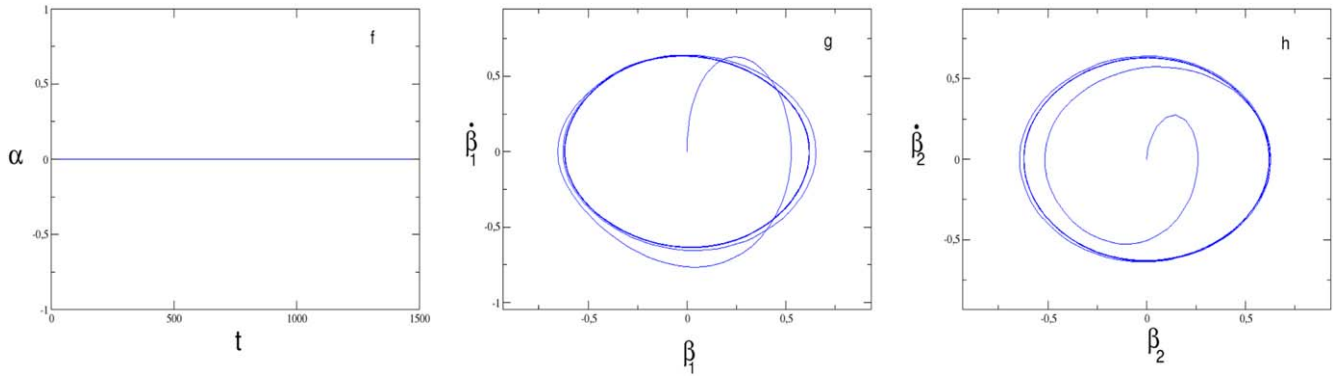

Figure 28. f: time histories of the oscillations of the micro-beam; g: phase difference phase space of the first Josephson junction; h: phase difference phase space of the second Josephson junction; $\omega_0 = 1$; $i_{G_0} = 2; J_1 = 1; J_2 = 3; J_3 = -1.6; J_4 = 0\varphi_{0_1} = 1; \varphi_{0_2} = 0.5; \sigma_1 = 1; \sigma_2 = 2; \sigma_3 = 1; \sigma_4 = 0; \varepsilon_1 = 1.7; \varepsilon_2 = 0.9; \varepsilon_3 = 0$.

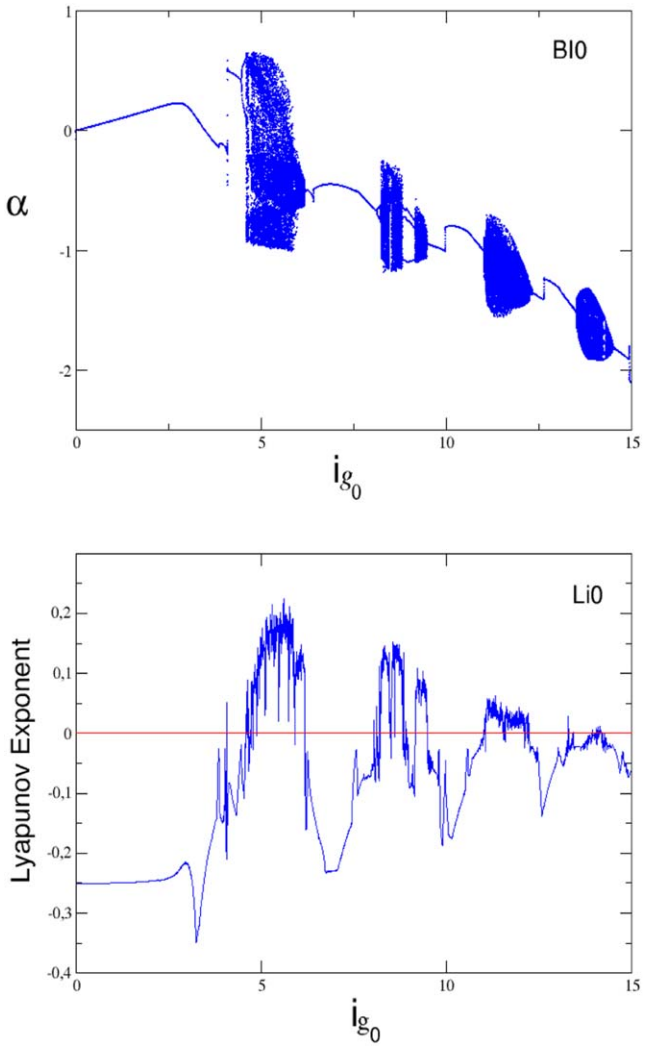

Figure 29. BI0: bifurcation diagram; Li0: Lyapunov exponent; $\omega_0 = 1$; $J_1 = 1$; $J_2 = 3$; $J_3 = -1.6$; $J_4 = 2$; $\varphi_{0_1} = 1$; $\varphi_{0_2} = 0.5$; $\sigma_1 = 1$; $\sigma_2 = 2$; $\sigma_3 = 1$; $\sigma_4 = 2$; $\varepsilon_1 = 1.5$; $\varepsilon_2 = 0.9$; $\varepsilon_3 = 0.5$.

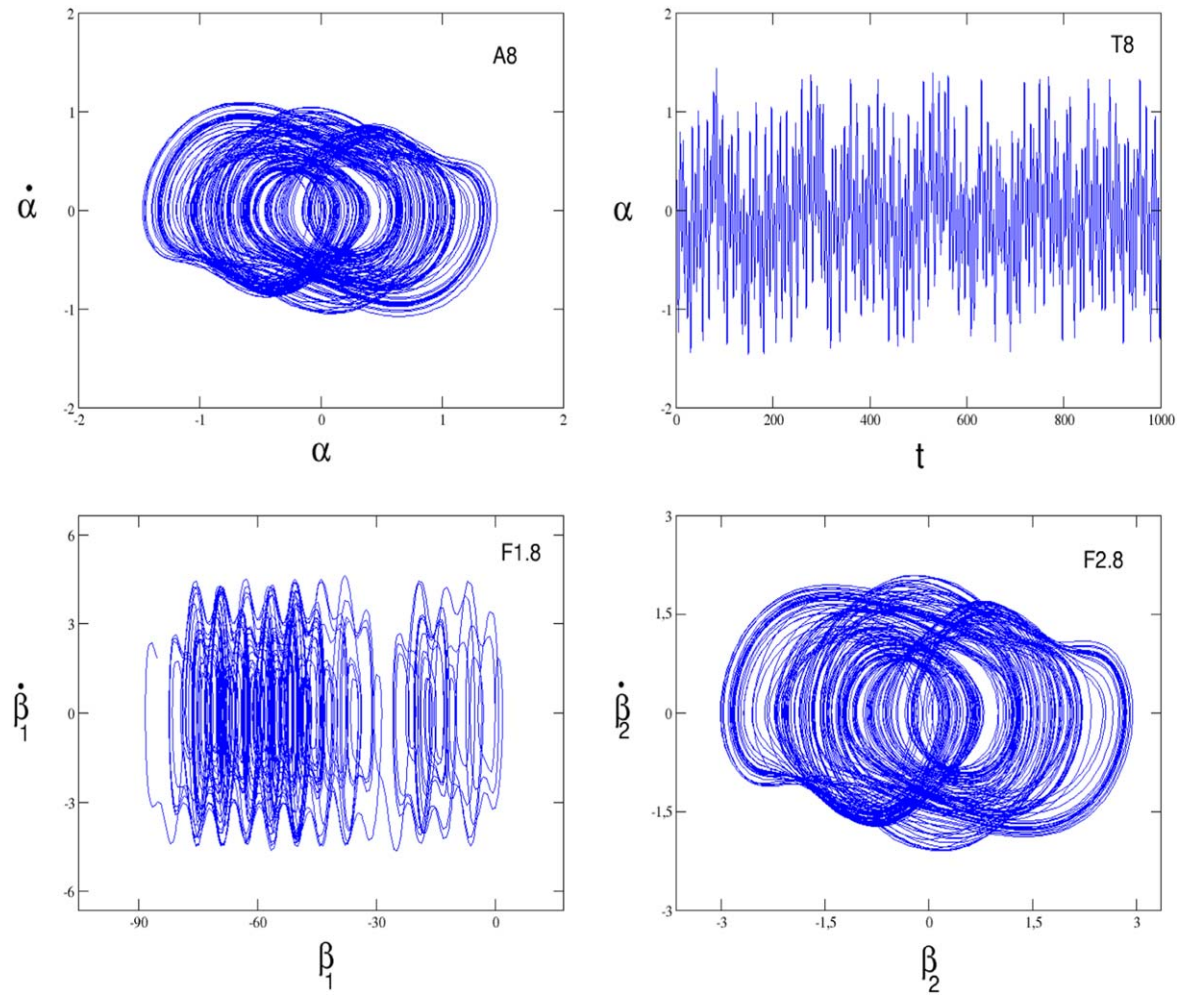

Figure 30. A_8: phase space of the flexural vibration of the micro-beam; T_8: time histories of the oscillations of the micro-beam; $F1_8$: phase difference phase space of the first Josephson junction; $F2_8$; phase difference phase space of the second Josephson junction: $\omega_0 = 1$; $i_{G_0} = 5.45$; $J_1 = 1$; $J_2 = 3$; $J_3 = -1.6$; $J_4 = 2\varphi_{0_1} = 1$; $\varphi_{0_2} = 0.5$; $\sigma_1 = 1$; $\sigma_2 = 2$; $\sigma_3 = 1$; $\sigma_4 = 2$; $\varepsilon_1 = 1.5\varepsilon_2 = 0.9$; $\varepsilon_3 = 0.5$.

Acknowledgments

G Koudafokê thanks IMSP-UAC and DAAD for financial support. The authors thank Professor Réné Yamapi for his suggestions. We would also like to thank very much the anonymous referees whose useful criticisms, comments and suggestions have helped strengthen the content and the quality of the paper.

ORCID iDs

C H Miwadinou https://orcid.org/0000-0001-9369-9583

References

[1] De Grave A 2004 Conception intégrèe des systèmes micro-électro-mécanique *Thèse de Doctorat Génie industriel* Institut National Polytechnique de Grenoble, France pp 37–47

[2] Grayson A, Shawge R C R, Johnson A S, Flynn N M, Yawen T, Michael L J C and Langer R 2004 *Bio MEMS Rev.* **92** 6–21

[3] Bullard E C, Li J, Lilley O R, Mulvanet P, Roukes M L and Sader J E 2014 *Phys. Rev. Lett.* **112** 015501

[4] Ekinci K L and Roukes M L 2005 *Rev. Sci. Instrum.* **76** 061101

[5] Etaki S, Poot M, Mahboob I, Onomitsu K, Yamgushi H and Van Der Zant H S J 2008 *Nat. Phys.* **4** 1057

[6] Herrera-May A L, Aguilera-cortés L A, García-Ramirez P J, Plascencia-Mora H and Torres-Cisneros M 2010 *Microsyst. Technol.* **16** 2067–74

[7] Karabalin R B, Cross M C and Roukes M L 2009 *Phys. Rev.* B **79** 165309

[8] Kozinsky I A, Postma H W C, Kogan O, Husain A and Roukes M L 2007 *Phys. Rev. Lett.* **99** 207201

[9] Matheny M H, Matt G L G, Villanueva R B and Karabalin M C 2014 *Nonlinear Dyn.* **89** 97–113

[10] Domguia S U, Abobda L T and Woafo P 2015 *J. Comput. Nonlinear Dyn.* **11** 051006

[11] Kwuimy C A K and Woafo P 2010 *J. Comput. Nonlinear Dyn.* **5** 021010

[12] Abdel Salem F and Shankar Sastry S 1983 *The Complete Dynamics of the Forced Josephson Junction Circuit: The Regions of Chaos* UCB/ERL M83/69 ECS Department, University of California, Berkeley

[13] Salem F M and Sastry S 1984 *Proc. IEEE ISCAS 1984b*
[14] Abidi A A and Chua L O 1979 *Electr. Circuits Syst.* **3** 186–200
[15] Ben-Jacob E, Goldhirsch I, Imry Y and Fishman S 1982 *Phys. Rev. Lett.* **49** 1599–602
[16] Belykh V N, Pedersen N F and Soerensen O H 1977 *Phys. Rev.* B **16** 4853–71
[17] Valkering T P, Hooijer C L A and Kroon F M 2000 *Physica* D **135** 137–53
[18] Nuznetsov A P, Sataev I R and Sedova Y V 2018 *J. Non Appl. Nonlinear Dyn.* **7** 1
[19] Yamapi R, Chabi Orou J B and Woafo P 2003 *Phys. Scr.* **67** 269–75
[20] Yamapi R and Filatrella G 2014 *Phys. Rev.* E **89** 052905
[21] Nayfeh A H and Mook T 1995 *Nonlinear Oscillations* (New York: Wiley)
[22] Bartuccelli M, Gentile G and Wright J A 2016 *Chaos* **26** 083108
[23] Enjieu Kadji H G, Nana Nbendjo R B, Chabi Orou J B and Talla P K 2007 *Phys. Plasmas* **15** 1–14
[24] Enjieu Kadji H G, Chabi Orou J B and Woafo P 2008 *Phys. Scr.* **77** 025503
[25] Miwadinou C H, Hinvi L A, Monwanou A V and Chabi Orou J B 2017 *Nonlinear Dyn.* **88** 97–113
[26] Chang T P 2017 *Math. Problems Eng.* **2017** 3769870
[27] Zebrowski J J, Grudzinski K, Buchner T, Kuklik P, Gac J, Gielerak G, Sanders P and Baranowski R 2007 *Chaos* **17** 015121
[28] Salem F M, Sastry S, Njah A N, Kayode O and Gboyega A A 2010 *Physica* C **470** 558564
[29] Giner de Haro J J 2012 Development of microelectromechanical systems for RF signal processing *PhD thesis* Universitat Autonoma de Barcelona, Spain
[30] James Blackburn A, Gregory Baker L and Smith H J T 2000 *Phys. Rev.* B **62** 5931
[31] Roukes M 2001 *Physics World* **14** 25–31